Technische Universiteit
Eindhoven
University of Technology

Department of Mechanical Engineering
Dynamics and Control

Model uncertainty in the indirect measurement of contact forces for a robotic manipulator

Master's Thesis

F.J.M. van Kuijk, BSc

Supervisor:	Prof.dr. H. Nijmeijer
Members:	dr. A. Saccon dr. ir. M.J.G. van den Molengraft
Advisor:	dr. ir. C.J.M. Heemskerk

DC 2016.089

Eindhoven, November 2016

Abstract

Force control of robotic manipulators is in general desired to let a robot execute an advanced task in which the robot is required to interact with the environment. In order to reduce costs, as well as the total mass of the system, it would be valuable if the contact forces of the robotic manipulator with the environment could be estimated.
In this project, a simulator has been developed for the purpose of studying the influence of parameter uncertainty on the accuracy of the contact force estimation. The residual contact force estimation method for a robotic manipulator is considered, which needs a model of the robot, information on the control torques, the joint positions and velocities in order to estimate the contact force. Because the method uses a model of the robot, parameter uncertainties are influencing the contact force estimation. Since joint friction will most likely play a big role in the parameter uncertainty, a study to the influence of the joint friction on the performance of the residual method has been done through simulations, for a robotic manipulator with 7 degrees of freedom. This is done for a task in which the robot mimics the motion of the wiping of a surface, in which it is required to estimate the contact forces while the robot is moving. The contact forces are thus estimated while the robot is performing the task. For the purpose of verification of the contact force estimation, a force plate has been realized which is able to measure contact forces using a 6-DOF force torque sensor.
It has been observed that the joint trajectory influences the accuracy of the residual method. The sensitivity to parameter uncertainty in the Coulomb joint friction differs for each joint and is dependent on the trajectory. A calibration procedure showed that the force plate is able to measure contact forces in z-direction for a static experiment. The measurement errors of the force plate have been observed to be much smaller than the error in the contact force estimation due to parameter uncertainty that can be noticed in the simulations.

Contents

List of Figures

List of Tables

Chapter 1

Introduction

Robots play a big role in our lives and this role is only increasing every day. Where in the past robots were mainly used in the industry, they begin to emerge more and more in domestic life. An example of robots in domestic life that are used in practice already are aid assisting robots in the healthcare sector, where these robots are helping the elderly with basic tasks. For these type of robots it is essential they can interact with their environments in which force control plays a big role, and although these robots are already used in practice, there is still a lot of research and development needed in this field.
This Masters thesis covers the research conducted in the field of contact force estimation for robotic manipulators. It mainly covers a study of the residual contact force estimation method, and in particular the sensitivity of the contact force estimation with respect to parameter uncertainties in the Coulomb joint friction for which multiple simulations are conducted. Furthermore, it covers the design and realization of a force plate which can be used for verification purposes and for experiments in further research.

1.1 Background

Force control of robotic systems is an important and interesting topic in modern day robotics, and is of great importance in the generally more advanced robotic applications. Where it is sufficient for simple tasks to use purely position control, it is often needed to use force control for more advanced tasks in which the robotic system's end effector is required to interact with the environment. These more advanced tasks can vary from applying a certain force to objects in the environment, to wiping a surface. One could also think of several machining and processing tasks such as the grinding and deburring of objects, and the posibility of realizing controlled contacts between the robotic end effector and the environment [1].
Besides tasks in which the environment has to be interacted with or in which objects have to be manipulated, force control can also be of great important for safety purposes. The control framework as proposed in [2], describes the physical collaboration between a human person and robotic system as three nested layers of consistent behaviors that the robot must guarantee and accomplish, with safety, coexistence and collaboration in order of importance. Specific situations could involve the collaboration or coexistence between a human person and a robotic system in the same working environment. To ensure a safe working environment and to prevent damages to the robot system itself, it is important to be able to detect external forces and to react to these forces in an appropriate way, for which force control is of essential importance.

In order to realize force control of a robotic system it is first required to determine the applied force at the end effector. This problem could be solved by mounting a force sensor in the robotic system which gives force feedback during operation. The accuracy of the force feedback when using a sensor method would be dependent on the accuracy of the force sensor itself. One can

implement any sensor that reaches the desired accuracy, although in general it will hold that higher accuracies lead to higher financial costs. A second possibility to solve this problem would be to implement a contact force observer to obtain an estimation of the contact force. In this way, a virtual force sensor is realized that can be used to get contact force feedback.

1.2 Motivation

Even though the use of physical force sensors generally leads to more accurate force feedback, using them also has certain downsides. The addition of an extra physical component to a robotic system leads to extra difficulties in the overall design of the arm and extra mass will simply be added to the system. Therefore, it would be interesting to determine if it is possible to realize a contact force observer that can obtain accurate enough results in order to be used as force feedback for the purpose of implementing force control in a robotic system.
An advantage of this method is that the dynamical properties of the system remain unaltered because no extra mass is added. Another advantage of contact force estimation are the lowered financial costs. Implementing and testing the virtual force sensor would logically take some time but the costs of purchasing a force sensor would be completely absent. These type of sensors can easily run up to multiple thousands of euros. By estimating the contact force a great amount of financial resources would be saved which could lead to a lower production cost for robotic systems in general.
The contact force estimation method that has been addressed in this report is the residual method as described in [3]. This method has already shown to deliver promising results in experiments. Besides this, the residual method only requires knowledge of the control torque, joint trajectories and velocities and a model of the robot. This information is very accessible in general, and only acquiring a model of the system provides the biggest challenge. For this reason the effect of parameter uncertainty is subject to research in this report. Search of relevant literature regarding the residual method, yielded only articles in which force estimation is addressed in case the robot is kept static. It is therefore interesting as well to determine how the residual method performs in a dynamic case in which the robot has to perform a certain task. The robot that will be used in this research is the ULNA manipulator which can be seen in figure 1.1. This robot is designed to mimic a human arm with a shoulder, elbow and wrist and has 7 degrees of freedom.

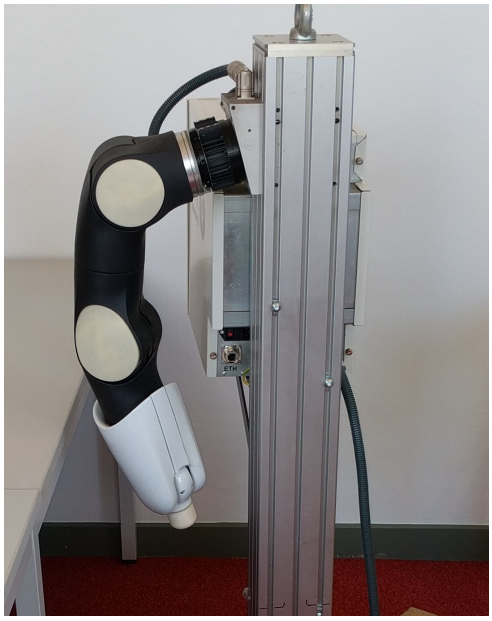

Figure 1.1: ULNA robotic manipulator

After implementing a contact force estimation method in a real robot, it is essential to verify the estimation. In order to do this, a force plate is designed which is able to measure 3D contact forces on a horizontal plate. Several force plates are already commercially available but are often expensive. For this reason, a 6-DOF force/torque sensor that's already in the possession of the TU Eindhoven has been used to realize the force plate.

1.3 Problem Statement

The problem statement of this project is divided in two parts, with the first part defined as:

Implement the residual method in matlab by using the mathematical model of the ULNA robotic manipulator to determine the sensitivity of the contact force estimation with respect to parameter uncertainties in the Coulomb joint friction

With the assumptions that

- the contact point is assumed to be a contact point with known position
- the joint positions and joint torques are known
- the contact surface is static, flat and horizontal and with a known properties and position in space

The second part can be defined as

Design and build a force plate that is able to measure and verify the estimated contact forces

with the requirements that

- it should be able to measure contact forces in all three Cartesian dimensions

1.4 Outline

The outline of this report is as follows. In chapter 2, contact force estimation by using the residual method is discussed. In chapter 3, the modeling of the robotic manipulator and the simulation environment are addressed. The realization of a force plate will be discussed as well together with an initial calibration procedure. In chapter 4 the results of the sensitivity study on the sensitivity of the residual method to parameter uncertainty are addressed. Lastly, in chapter 5, conclusions and recommendations for future research will be given.

Chapter 2

Contact force estimation using the residual method

In this chapter a literature review on contact force estimation will be presented. First, literature covering contact force estimation in general will be addressed after which literature regarding the residual method discussed. Subsequently the mathematical description of the robot and the residual method will be presented.

2.1 Literature review

2.1.1 Contact force estimation in general

Different estimation methods can be used to estimate the contact force of the robotic arm and the environment. The method presented in [18] relies on the possibility to detect or estimate the torques in the joints and the availability of motor current measurements. Force estimation is obtained by compensating for torque induced by friction and torques that are needed to keep the robotic arm at a certain position, in which the friction is modeled as a combination of Coulomb and viscous friction models whose coefficients are determined with a heuristic approach. The total torque is determined by using the torque constant vector and armature currents from the motors. By inverting the geometric Jacobian, an estimation of the contact wrench, the union of the contact force and torque, can directly be computed when the joint torques that are exerted by the environment are known, using the forward kinematics.
The method of [19] is based on detuning of the low-level joint control loops. After starting with an aggressive tuning rule, detuning will result in a more stable and robust controller by changing the control gains at the expense of performance. The forces are estimated from the joint position control errors. The proposed method shows that when a priori information about the external torques is known, the contact force can be estimated when they are assumed to be small.
In [20], an algorithm is proposed to estimate the external forces that are exerted on the end-effector of a robot manipulator. This method uses information from the joint torque sensors and is a combination of Time Delay Estimation and input estimation with the external force considered as an unkown input. Based on the time delayed signals of the system variables, the current system behavior is being estimated. A big advantage of this algorithm is that it does not require an accurate dynamical model of the robotic arm. Results obtained from simulations show that this method is able to estimate the contact forces with small errors.
In [21], the authors present a method which reconstructs the external forces an torques from motor currents/torques and joint angles which is demonstrated by performing measurements obtained from a ABB Dual-Arm Concept Robot. The method compensates for joint friction with a Coulomb and viscous friction model and computed joint speeds after which the effective motor torques are determined. Friction identification has to be performed to obtain accurate parameters. By

knowing the inverse of the Jacobian matrix for the current pose, the contact forces can then be estimated. By including prior knowledge or assumptions on the disturbance torques and contact forces a Bayesian approach is employed, in which it is key to tune covariance matrices after which the contact forces are obtained by the solution of an optimization problem. The authors present results for a static load case in which a force has been applied to the end effector in the z-direction, showing an accuracy of estimating the contact force in this direction of approximately 50%.

2.1.2 Contact force estimation with the residual method

The authors of [8], [3] and [9] propose the residual method. This method requires information of the joint positions, the applied control torque, and the dynamic model of the robotic arm in order to compute an estimation of the contact forces and torques. These forces can be estimated at any contact point of the robot, if the position of this contact point is known. The method obtains this estimation by computing the so called residual, which dynamic equation has a stable and first-order filter structure. The residual is approaching the torques exerted by the environment on the arm. By computing the inverse of the contact Jacobian by using the joint positions, an estimation of the contact forces and torques can be obtained. In 3, the authors have implemented the residual method on a KUKA LWR. The method is validated with experiments in which a constant load is applied to the arm. The authors present results that show an estimation of the contact forces with a maximum error of 5 percent. Although the method shows promising results for static load cases, results for a dynamic load case haven't been presented yet in literature to the best of our knowledge. It is therefore interesting to research the abilities of the residual method in estimating contact forces for a dynamic load case in which the contact forces are estimated while the robot is performing a task. Because this is an interesting topic, we research contact force estimation for a dynamic load case in this report.

2.2 Residual Method

2.2.1 Mathematical description of the robot

To simulate the dynamic behavior of the robot, the following model is considered

$$\mathbf{M}(\mathbf{q})\ddot{\mathbf{q}} + \mathbf{C}(\mathbf{q}, \dot{\mathbf{q}})\dot{\mathbf{q}} + \mathbf{g}(\mathbf{q}) = \tau_c + \tau_e(\mathbf{q}, \dot{\mathbf{q}}) + \tau_f(\mathbf{q}, \dot{\mathbf{q}}) \tag{2.1}$$

in which $\mathbf{M}(\mathbf{q})$ is the mass matrix, $\mathbf{C}(\mathbf{q}, \dot{\mathbf{q}})$ the coriolis matrix and $\mathbf{g}(\mathbf{q})$ the gravity vector. The joint positions are represented by $\mathbf{q}$ and its time-derivatives $\dot{\mathbf{q}}$ and $\ddot{\mathbf{q}}$ being respectively the joint velocity and joint acceleration. The control torque is represented by τ_c while τ_f represent the torque due to joint friction. The forces on the environment that act on the robot are represented by τ_e as

$$\tau_e = \mathbf{J}_c^T(\mathbf{q})\mathbf{F}_c \tag{2.2}$$

with $\mathbf{J}_c^T(\mathbf{q})$ the contact jacobian. Vector $\mathbf{F}_c$ represents the contact vector containing the forces and moments in the three cartesian directions and is given by

$$\mathbf{F}_c = \begin{bmatrix} F_x \\ F_y \\ F_z \\ M_x \\ M_y \\ M_z \end{bmatrix} \in \mathbb{R}. \tag{2.3}$$

2.2.2 Computation of the control torque

In order to compute the required control torque $\tau_\mathbf{c}$ for a desired trajectory, equation (2.1) is taken and rewritten as

$$\tau_c = \mathbf{M}(\mathbf{q})\ddot{\mathbf{q}} + \mathbf{C}(\mathbf{q}, \dot{\mathbf{q}})\dot{\mathbf{q}} + \mathbf{g}(\mathbf{q}) - \tau_e(\mathbf{q}, \dot{\mathbf{q}}) - \tau_f(\mathbf{q}, \dot{\mathbf{q}}) \tag{2.4}$$

It is now assumed to be known that all model parameters $\mathbf{M}(\mathbf{q})$, $\mathbf{C}(\mathbf{q}, \dot{\mathbf{q}})\dot{\mathbf{q}}$, $\mathbf{g}(\mathbf{q})$, $\tau_e(\mathbf{q}, \dot{\mathbf{q}})$ and $\tau_f(\mathbf{q}, \dot{\mathbf{q}})$ are known for simulation purposes. Although this is unrealistic to assume in reality, it can be assumed that these parameters are known for the purpose of testing the contact force estimation. By assuming these parameters are known, a control torque can be computed by knowing the joint trajectories. When the desired joint trajectories $\mathbf{q}_d$, $\dot{\mathbf{q}}_d$ and $\ddot{\mathbf{q}}_d$ are then substituted into equation 2.4, the control torque τ_c can be obtained.

2.2.3 Residual method

In order to estimate contact forces at the end effector of a robotic manipulator, the residual-based method of [8], [3] and [9] is considered. This method requires information about the dynamic model of the robotic arm, full information about the joint positions $\mathbf{q}$, joint velocities $\dot{\mathbf{q}}$ and control torque τ_c. The residual $\mathbf{r}(t)$ is defined as

$$\mathbf{r}(t) = \mathbf{K_i}\left[\mathbf{M}(\mathbf{q})\dot{\mathbf{q}} - \int_0^t (\tau_c + \tau_f + \mathbf{C}(\mathbf{q}, \dot{\mathbf{q}})^T - \mathbf{g}(\mathbf{q}) + \mathbf{r})ds)\right] \in \mathbb{R}^n \tag{2.5}$$

with $\mathbf{K_i}$ a diagonal gain matrix. Matrices $\mathbf{M}(\mathbf{q})$, $\mathbf{C}(\mathbf{q}, \dot{\mathbf{q}})$ and gravity vector $\mathbf{g}(\mathbf{q})$ can be obtained from the mathematical model of the manipulator.

To show that the residual approaches the value of the external applied torque, the residual as it is defined in (2.5) is differentiated with respect to time

$$\dot{\mathbf{r}}(t) = \mathbf{K_i}\left[\dot{\mathbf{M}}(\mathbf{q})\dot{\mathbf{q}} + \mathbf{M}(\mathbf{q})\ddot{\mathbf{q}} - \tau_c - \tau_f - \mathbf{C}^T(\mathbf{q}, \dot{\mathbf{q}})\dot{\mathbf{q}} + \mathbf{g}(\mathbf{q}) - \mathbf{r}\right] \tag{2.6}$$

Due to the skew symmetric property of the term $\dot{\mathbf{M}}(\mathbf{q}, \dot{\mathbf{q}}) - 2\mathbf{C}(\mathbf{q}, \dot{\mathbf{q}})$, which is explained in [17], the derivative of the mass matrix with respect to time can be expressed as

$$\dot{\mathbf{M}}(\mathbf{q}) = \mathbf{C}(\mathbf{q}, \dot{\mathbf{q}}) + \mathbf{C}^T(\mathbf{q}, \dot{\mathbf{q}}) \tag{2.7}$$

which is equivalent to the term $\dot{\mathbf{M}}(\mathbf{q}, \dot{\mathbf{q}}) - 2\mathbf{C}(\mathbf{q}, \dot{\mathbf{q}})$ being skew-symmetric. Equation (2.6) is rewritten by substituting the expression for $\dot{\mathbf{M}}(\mathbf{q})$ given in (2.7) into it, yielding

$$\dot{\mathbf{r}}(t) = \mathbf{K_i}\left[(\mathbf{C}(\mathbf{q}, \dot{\mathbf{q}}) + \mathbf{C}^T(\mathbf{q}, \dot{\mathbf{q}}))\dot{\mathbf{q}} + \mathbf{M}(\mathbf{q})\ddot{\mathbf{q}} - \tau_c - \tau_f - \mathbf{C}^T(\mathbf{q}, \dot{\mathbf{q}})\dot{\mathbf{q}} + \mathbf{g}(\mathbf{q}) - \mathbf{r}\right] \tag{2.8}$$

in which it can be seen that the two transposed coriolis terms $\mathbf{C}^T(\mathbf{q}, \dot{\mathbf{q}})$ cancel each other. This results in

$$\dot{\mathbf{r}}(t) = \mathbf{K_i}\left[\mathbf{M}(\mathbf{q})\ddot{\mathbf{q}} + \mathbf{C}(\mathbf{q}, \dot{\mathbf{q}})\dot{\mathbf{q}} + \mathbf{g}(\mathbf{q}) - \tau_c - \tau_f - \mathbf{r}\right] \tag{2.9}$$

From (2.1), we have

$$\tau_e = \mathbf{M}(\mathbf{q})\ddot{\mathbf{q}} + \mathbf{C}(\mathbf{q}, \dot{\mathbf{q}})\dot{\mathbf{q}} + \mathbf{g}(\mathbf{q}) - \tau_c - \tau_f \tag{2.10}$$

and therefore (2.10) is simply equal to the first-order filter structure

$$\dot{\mathbf{r}}(t) = \mathbf{K}_i(\tau_e - \mathbf{r}) \tag{2.11}$$

Due to the negative eigenvalues of matrix $\mathbf{K}_i$ in (2.11), the observer is stable and will converge exponentially to $\mathbf{r} = \tau_e$ in the case this external torque τ_e is constant over time. If τ_e is varying

the residual $\mathbf{r}$ will thus approach the external applied torque τ_e after a finite amount of time depending on the magnitude of diagonal gain matrix $\mathbf{K_i}$.

Using (2.5) the estimated contact force $\hat{\mathbf{F}}_c$ is computed as

$$\hat{\mathbf{F}}_c = (\mathbf{J}_c^T(q))^{\#}\mathbf{r} \tag{2.12}$$

with $\mathbf{J}_c$ the contact Jacobian, which is known since it is assumed that contact takes place exactly at the end-effector frame. The # symbol denotes a pseudoinverse which is necessary due to the matrix $\mathbf{J}_c$ not being square. This is implemented as a Moore-Penrose pseudoinverse of the Jacobian $\mathbf{J}_c^{\#}$, which can be computed as

$$\mathbf{J}_c^{\#} = \mathbf{J}_c^*(\mathbf{J}_c\mathbf{J}_c^*)^{-1} \tag{2.13}$$

in which $\mathbf{J}_c^*$ is the conjugate transpose of the contact jacobian.

2.3 Summary

In this section, a short literature review regarding contact force estimation is addressed. Literature on force estimation are discussed which present promising results in static load cases. Literature on contact force estimation for dynamic load cases has not been found, and is therefore an interesting topic to research. The mathematical description of the robot is discussed and the residual method is presented. It is shown that the residual, indeed approaches the external applied torque.

Chapter 3

A simulation environment for studying the sensitivity of the residual method

This chapter will describe the robotic manipulator used in this research. The simulation environment that has been created will be discussed in the first part. This includes visualization, modeling of the environment and the generation of reference trajectories with the goal to obtain a tool to study the sensitivity of the residual method. The second part will address the realization of a force plate, which is created for the purposes of validation of contact force estimation. A summary will be given at the end of this chapter.

3.1 Simulator

3.1.1 Robotic manipulator

The robotic manipulator that will be considered for this research is shown in figure 1.1. This arm is carrying the name ULNA and is built by PAL robotics [4]. It has 7 degrees of freedom and is mimicking the human arm with a shoulder, elbow and wrist. Since it is not equipped with a force sensor it would be useful for the arm be able to estimate contact forces. The dimensions of the ULNA arm are indicated by the letters in figure 3.1, with A = 620mm, B = 150 mm, C = 280 mm. The mass of the arm is equal to 9 kg and the arm has a payload of a maximum of 1 kg. In this figure the joints are indicated with the numbers 1 to 7.
In order to compute the dynamics and forward kinematics, the open-source iWholeBodyModel interface [5] is used. This interface is able to compute the mass matrix $\mathbf{M}(\mathbf{q})$, the coriolis vector $\mathbf{c}(\mathbf{q}, \dot{\mathbf{q}}) = \mathbf{C}(\mathbf{q}, \dot{\mathbf{q}})\dot{\mathbf{q}}$ and the gravity vector $\mathbf{g}(\mathbf{q})$ given that a URDF file is provided, containing the dynamic and kinematic information of the robot.

3.1.2 Visualization

In order to visualize the simulations and to clearly show the arm's trajectory, a simulator is created in Matlab to visualize the dynamic movements of the arm. The different orientation frames are indicated in the figure which will be clarified in Section 3.1.3 which treats the task specification. The visualization shows the contact surface with which the arm is interacting. The end effector trajectory is marked with a green and red trail line. This trail line is green when the end effector

of the arm is moving in free air. When the end effector makes contact with the environment, the trail line turns red. This can be observed by closely looking at the contact surface in figure 3.2.

Figure 3.1: ULNA joint numbers and general dimensions A = 620mm, B = 150 mm and C = 280

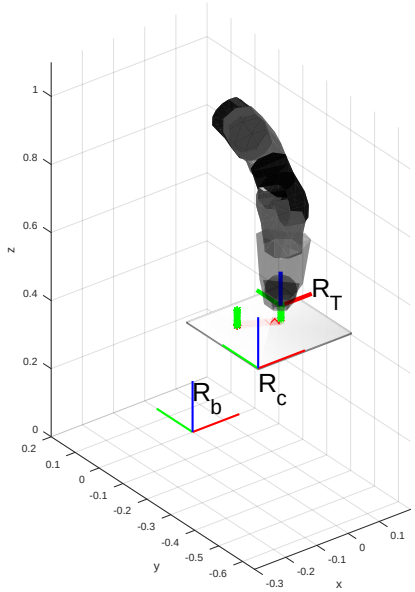

Figure 3.2: Visualization of a simulation

3.1.3 Modeling the environment

Task specification

The environment with which the arm will interact is modeled as a flat and static surface. An illustration of the environment is given in figure 3.3. The figure also shows the four different coordinate frames. The base frame R_B is located at the base of the robot and is selected as the world frame. The contact surface orientation is parameterized by the table frame R_T. The end effector frame R_E is placed at the center of the end effector of the arm. The contact frame R_C has the location of the end effector frame R_E but the orientation of the constraint frame R_C. This allows for an easy and straightforward description of the task.

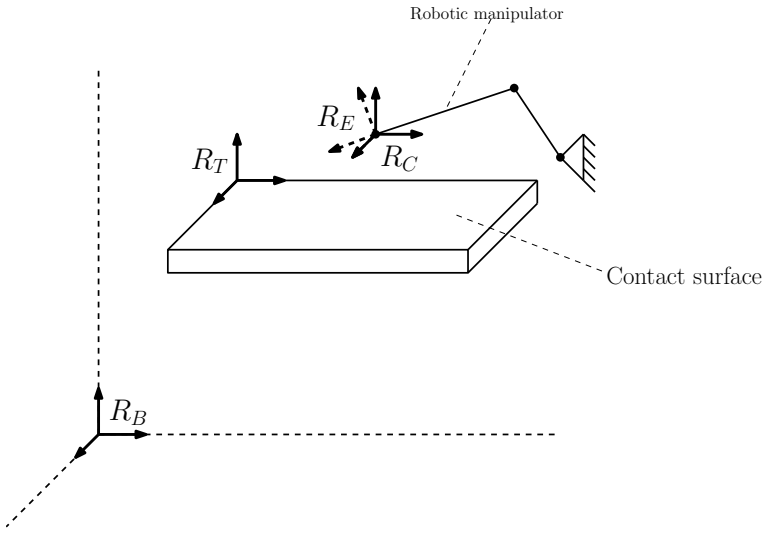

Figure 3.3: Schematic illustration of the location of the coordinate frames

The task of the robot is defined in such a way, that it resembles the wiping of a surface. After the end effector ascends until it is at the same height as the surface, it starts interacting with it. The task of the robot is to control the force in the direction that is normal to the surface. Meanwhile it is required to control the position in the plane that is parallel to the surface.

Normal force

A contact of the end effector perpendicular to the surface will result in a normal force $F_n(t)$. This force is modeled as proposed by Hunt and Crossley [12], ensuring a smooth transition when the end effector comes into contact with the surface. This model can be described as

$$F_n = kx_p^\alpha + \lambda x_p^\alpha v_e^n \tag{3.1}$$

in which the first term is an elastic component and the second term a dissipative component. In (3.1), the penetration of the table is represented by x_p. The parameter k is the spring constant and exponent α depends on the local geometry around the contact area. The force damping weight is represented by λ. The end effector velocity in the direction normal to the surface is represented by v_e^n, defined with respect to the table frame.

Contact friction

The contact forces $F_f(t)$ due to the friction of the surface are modeled as a combination of Coulomb and viscous friction [10]. This model can be written as

$$F_f = \mu_s F_n sign(v_e^n) + \mu_k v_e^p \tag{3.2}$$

with μ_s and μ_k the static friction and kinematic friction coefficients respectively. Since the end effector of the ULNA arm is made of a polymer, the values for the frictions coefficients are set to $\mu_s = 0.4$ and $\mu_k = 0.3$ which corresponds with a contact between plastic and metal [11]. The normal force with which the end effector interacts with the surface is represented by F_n and is the same as in (3.1). The end effector velocity in the direction normal to the surface is represented by v_e^n, while v_e^p is the end effector velocity that is parallel to the surface. Both velocities are defined with respect to the table frame.

3.1.4 Joint friction model

To allow the residual method to take into account joint friction, (2.5) is modified into

$$\mathbf{r}(t) = \mathbf{K_i}\left[\mathbf{M}(\mathbf{q})\dot{\mathbf{q}} - \int_0^t (\tau_c + \tau_f + \mathbf{C}(\mathbf{q},\dot{\mathbf{q}})^T - \mathbf{g}(\mathbf{q}) + \mathbf{r})ds)\right] \in \mathbb{R}^n \tag{3.3}$$

where τ_f denotes the joint friction torque. This torque is modeled as a combination of Coulomb and viscous friction according to the model in [13], which is defined as

$$\tau_f = sign(\dot{\mathbf{q}})\mu_c + \mu_v\dot{\mathbf{q}} \tag{3.4}$$

with μ_c the Coulomb friction parameter and μ_v the viscous friction parameter which will be assumed to be the same for all joints. In [14], estimated Coulomb and viscous friction parameters are given for a DLR medical robot while in [15] these parameters are given for the mitsubishi PA10-6CE manipulator. Since the model identification of the ULNA arm is not within the scope of this project, the joint friction parameters are set to a value in the same order of magnitude as in the literature that is mentioned above. To validate the used friction coefficients, we have performed several measurements in which a torque is applied to the static joints by applying a force with spring Newton-meter at a certain distance of the joint. The moment the joint starts moving is the point where the static friction is exceeded. In that case, the spring Newton-meter displays the required force that was needed to accomplish exceeding the Coulomb friction. The value for the Coulomb friction coefficient is thus set to $\mu_c = 3$ [Nm]. The viscous parameter is set to the same value as $\mu_v = 3$ [Nms/rad] for all joints since [15] shows values in the same order of magnitude for μ_c and μ_v.

3.1.5 Computation of the reference trajectory

In order to control the position and orientation of the end-effector, the desired end effector position x_d needs to be prescribed with respect to time. This position is defined in the contact frame R_c shown in figure 3.2. To obtain the joint trajectories the inverse kinematics then must be solved. Obtaining an algebraical solution of the Inverse Kinematics for a 7-DOF manipulator can computationally be a challenging task. In order to obtain the joint positions as a function of the end effector position, the Jacobian inverse technique is used. The algorithm for this technique is listed below.
The first step is the initialization step, which involves setting the joint state iteration vector $\vec{\theta}_{it}$ to zero. The position difference vector $\Delta\vec{x}$ is initialized as the difference between the current position and the desired final position. The threshold value ϵ has set to the value that achieves the desired accuracy of the reference trajectory. After the initialization, a while loop can be started to obtain the approximate solution to the Inverse Kinematics. The end effector position $\vec{x}_{it}$ is computed with the forward kinematics, after which the position difference vector $\Delta\vec{x}$ can be computed when the desired position $\vec{x}_d$ is known. To compute the joint state difference vector $\Delta\vec{\theta}$, the inverse jacobian J^+ must be known. Since we are dealing with a 7-DOF system, the jacobian will be non-square which will make direct inversion not possible. As a solution, the MoorePenrose inverse is used, computing a pseudoinverse of the jacobian matrix. When the joint state difference vector

Algorithm 1 Jacobian inverse technique

1: **Initialize**
2: $\vec{\theta}_{it}$ ▷ Joint state iteration vector
3: $\Delta\vec{x}$ ▷ Position difference vector
4: ϵ ▷ Threshold value
5: **while** $|\Delta\vec{x}| > \epsilon$ **do**
6: $\quad\vec{x}_{it} = FK(\vec{\theta}_{it})$ ▷ Position iteration vector
7: $\quad\Delta\vec{x} = \vec{x_d} - \vec{x}_{it}$ ▷ Position difference vector
8: $\quad\Delta\vec{\theta} = J^{+}\Delta\vec{x}$ ▷ Joint state difference vector
9: $\quad\vec{\theta}_{it} = \vec{\theta}_{it} + \Delta\vec{\theta}$ ▷ Update joint state

is known, the state can be updated. The while loop is repeated until the the difference between the actual and desired end effector position is below a desired threshold value.

3.2 Force Plate

3.2.1 Motivation

After implementing the residual contact force estimation method on a physical robotic manipulator, it would be desirable to determine its quality and performance. An experimental validation is required to determine the accuracy and the convergence rate of the estimation in comparison to the real contact forces. When looking at certain cases in which the contact force estimation can be applied, one can differentiate between a static and a dynamic situation. In the static case, a robotic manipulator exercises a force on the environment while the manipulator remains static and thus has joint velocities equal to zero: $\dot{\mathbf{q}} = \mathbf{0} \in \mathbb{R}^{n\times 1}$, for a manipulator with n degrees of freedom. In the case of a dynamic situation, the robotic manipulator is in movement and thus has joint velocities unequal to zero: $\dot{\mathbf{q}} \neq \mathbf{0} \in \mathbb{R}^{n\times 1}$. An example of a dynamic situation is the task specification of wiping a table as discussed in section 3.1.

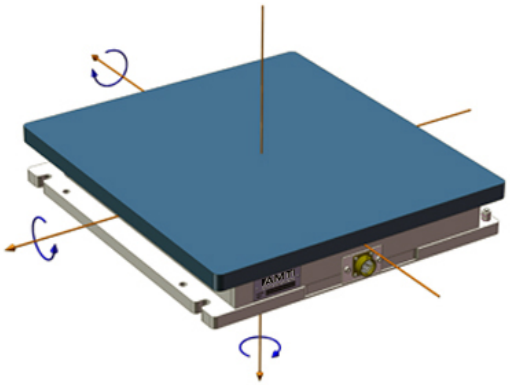

Figure 3.4: AMTI commercially available force plate, [6]

To measure contact forces for a static case is relatively easy: one could easily keep the manipulator at a fixed position while applying a known load at the end effector in a fixed direction. This could be achieved by attaching weights to the end effector. Measuring the contact forces for a dynamic case is less trivial and not as easy to accomplish. In order to measure contact forces in both a static and a dynamic situation of the manipulator, thea realization of a force plate will be described in this chapter. Force plates are already commercially available and are able to measure contact forces in all three cartesian directions. These devices can measure torques around the three principal axes, but only around the center of the force plate. Determining the contact torque is thus not possible over the whole area of the force plate. The main application for which these devices are used, is to analyze and research the gait of humans and animals. An illustration of a commercially available product can be seen in figure 3.5 showing an image of an AMTI force plate.
Although these devices are already commercially available they require a significant amount of economic resources, starting at approximately €10.000. Due to these high costs it is chosen to design and build a new force plate which can be used for verification of contact forces. To realize this new force plate, a 6 DOF force torque sensor in property of the TU/e is used. An image of this sensor is shown in figure 3.5.

3.2.2 Design specifications

The specifications of the 6 DOF force torque sensor can be seen in Table 3.1, containing information about the sensing range, resolution, and stiffness for all six degree of freedoms, together with the

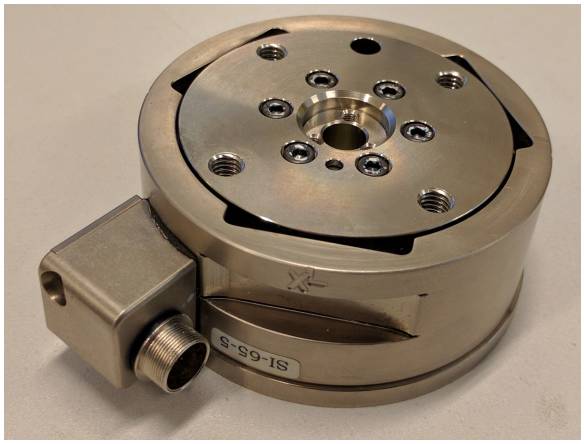

Figure 3.5: 6 DOF ATI force torque sensor

single-axis overload which indicates the maximum force the sensor can handle before it breaks. Notice that the sensing ranges are much smaller than the single-axis overload.

DOF	**Sensing range**	**Resolution**	**Single-axis overload**	**Stiffness**
F_x, F_y	± 65 [N]	0.0125 [N]	± 1200 [N]	$9.1 \cdot 10^6$ [N/m]
F_z	± 200 [N]	0.0250 [N]	± 4100 [N]	$1.8 \cdot 10^7$ [N/m]
T_x, T_y	± 5 [Nm]	$7.5 \cdot 10^{-4}$ [Nm]	± 79 [Nm]	$1.1 \cdot 10^4$ [Nm/rad]
T_z	± 5 [Nm]	$7.5 \cdot 10^{-4}$ [Nm]	± 82 [Nm]	$1.6 \cdot 10^4$ [Nm/rad]

Table 3.1: Specifications of the ATI 6 DOF force torque sensor

The design of the force plate will thus be dependent on the design of the 6 DOF force torque sensor. The sensing range and resolution of the force plate will also be limited by the specifications of this sensor. The specifications of the force plate should follow from the task specification of the robotic arm which is defined in chapter 3 as a wiping motion. Since the payload of the arm is 1 kg (approximately 10 N), it can be seen in table 3.1 that the specifications of the force torque sensor and in specific the sensing ranges are sufficient by a large margin. For the purpose of future research this can be useful for measuring contact forces that are bigger than 10 N.

The desired design specifications are listed below.

- The length and width L and W of the force plate are set to 300 mm, providing a combination of a decent workspace and compactness.
- The desired degrees of freedom in which the contact force can be determined are F_x, F_y and F_z. Besides these, the force plate should to be able to measure the contact torque T_z in some cases.
- The desired sensing ranges for F_x, F_y and F_z should at least be able to handle a maximum payload of the arm of 1 kg, equivalent to approximately 10 N.
- The desired resolution of the force plate is directly limited by the resolution of the 6 DOF force torque sensor. Due to measurement noise and due to the fact that the specifications for the 6 DOF force torque sensor are given for optimal conditions, the resolutions as stated in table 3.1 are unlikely to be reached. Therefore, we define the desired accuracy of the force plate as 1% of the maximum payload.

An overview of the desired specifications of the force plate can be seen in Table 3.2.

Specification	**Symbol**	**Quantity**	**Dimension**
Dimensions	$L \times W \times h$	$300 \times 300 \times 10$	[mm]
Measured contact-DOF	F_x, F_y, F_z, T_z		[N]
Sensing Range (minimum)	F_x, F_y	± 10	[N]
	F_z	± 10	[N]
	T_z	± 1	[Nm]
Accuracy	F_x, F_y	0.1	[N]
	F_z	0.1	[N]
	T_z	0.01	[Nm]

Table 3.2: Force plate design specifications

3.2.3 Design of the force plate

The force plate is designed with one 6 DOF force torque sensor. A top and bottom view of the sensor can be seen in figure 3.6. Notice the indication of 4 bolt holes on both the top and bottom of the sensor, providing the possibility of mounting it onto another object and mounting another object on the sensor.

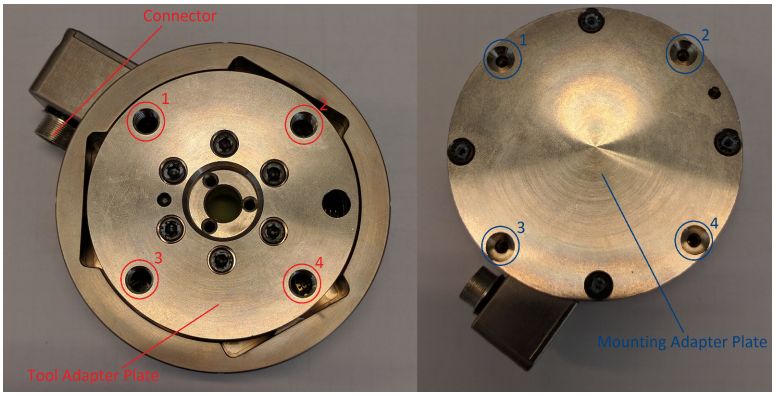

Figure 3.6: F/T Sensor: top and bottom view

The design of the force plate consists of a top and a bottom plate, with the force torque sensor bolted in between. A schematic picture of the top plate can be seen in figure 3.7 with in the left side of the figure the front view of the design, and at the right side showing the top view. The sensor is indicated with red while the bolts are indicated with blue. Optional cover plate holes are visible in this figure but are currently not present in the design.
The top plate has length L, width W and height h. The top plate is bolted onto the sensor with four M6 bolts through the sensor mounting holes.
The bottom plate has length L_b, width W_b and height h_b. A schematic picture of the bottom plate can be seen in figure 3.8, it has four holes with which the bottom plate can be bolted on the sensor. In figure 3.9 the complete design can be seen including an optional cover plate. The cover plate is currently not included but could easily be applied in the future to create the possiblity of changing the contact surface and thus its properties. The cover plate is attached to the top plate and is bolted onto the tool adapter plate of the sensor. The mounting adapter plate of the sensor attached with the bottom plate with four bolts after which the bottom plate is attached to the fixed world with clamps.

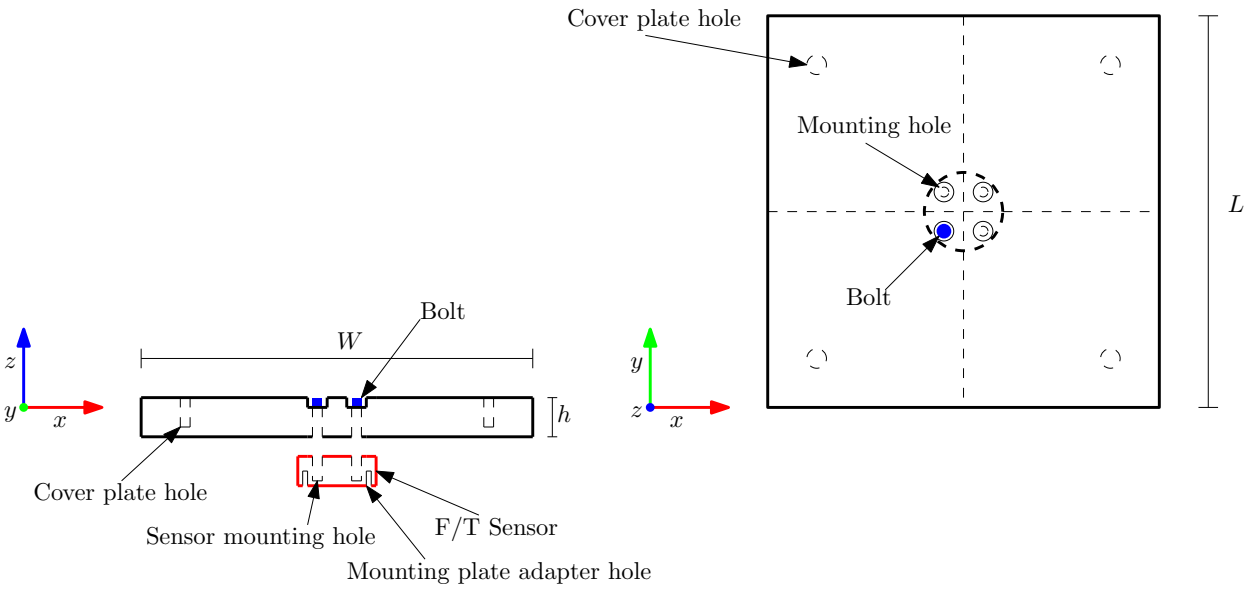

Figure 3.7: Schematic drawing of the top plate

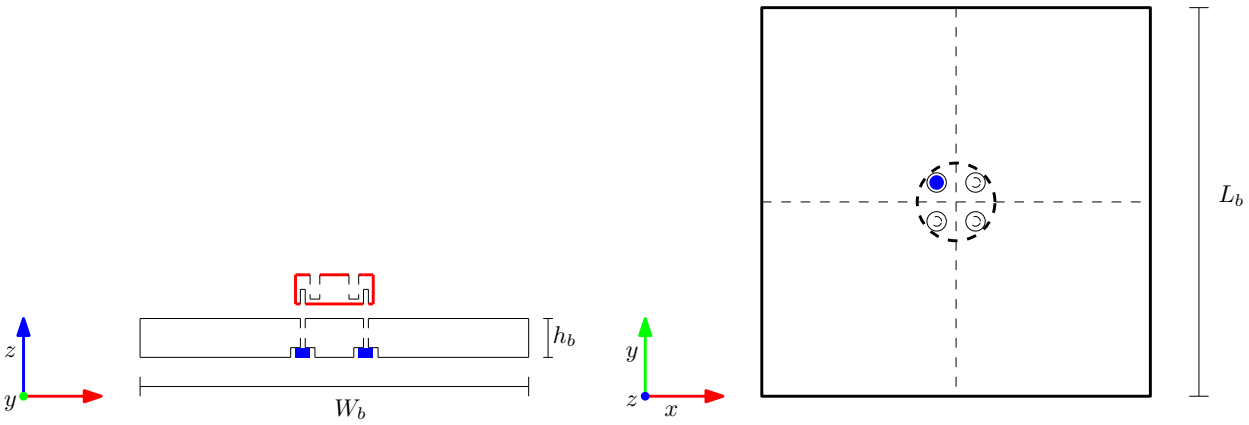

Figure 3.8: Schematic drawing of the bottom plate

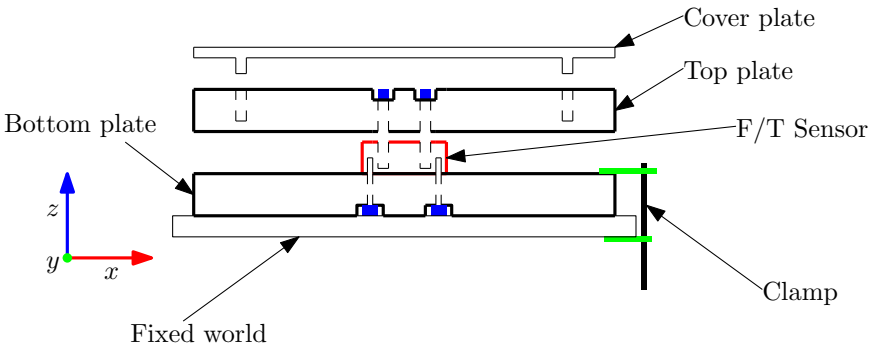

Figure 3.9: Schematic drawing of the front view of the design

In order to obtain an expression for the contact forces for this design, the equilibrium of forces and moments can be used to relate the measured sensor vector to the applied contact vector as

$$A_s \cdot_s \mathrm{f} =_c \mathrm{f}, \tag{3.5}$$

in which A_s is the sensor matrix, ${}_s\mathrm{f}$ the sensor vector and ${}_c\mathrm{f}$ the contact vector. When a point contact is assumed, ${}_s\mathrm{f}$ contains the forces and torques expressed in the three cartesian directions, defined as

$${}_s\mathrm{f} = \begin{bmatrix} {}_sf \\ {}_s\tau \end{bmatrix} = \begin{pmatrix} {}_sf_x \\ {}_sf_y \\ {}_sf_z \\ {}_s\tau_x \\ {}_s\tau_y \\ {}_s\tau_z \end{pmatrix} \in \mathbb{R}^{6x1} \tag{3.6}$$

The applied contact vector ${}_c\mathrm{f} \in \mathbb{R}^{6\times1}$ contains the applied contact forces and applied contact torques, and is defined as

$${}_c\mathrm{f} = \begin{bmatrix} {}_cf \\ {}_c\tau \end{bmatrix} = \begin{pmatrix} {}_cf_x \\ {}_cf_y \\ {}_cf_z \\ {}_c\tau_x \\ {}_c\tau_y \\ {}_c\tau_z \end{pmatrix} \in \mathbb{R}^{6\times1} \tag{3.7}$$

The sensor matrix A_s is defined as

$$A_s = \begin{bmatrix} I & O \\ R & I \end{bmatrix} \in \mathbb{R}^{6\times6} \tag{3.8}$$

with $I \in \mathbb{R}^{3\times3}$ representing the identity matrix and $O \in \mathbb{R}^{3\times3}$ the zero matrix.

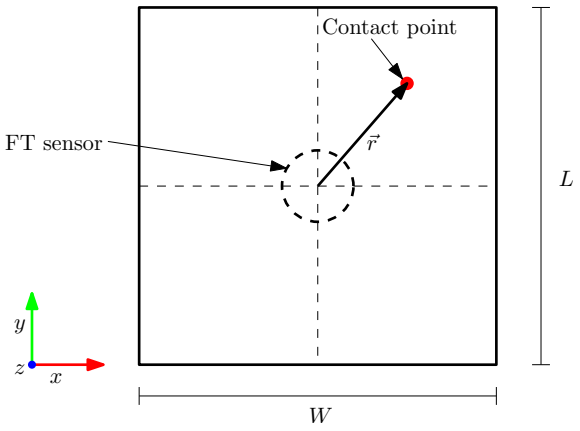

Figure 3.10: Contact point on force plate

Matrix $R \in \mathbb{R}^{3\times3}$ can be derived by writing the measured sensor torque as the cross product between position vector $\vec{r}$ as indicated in figure 3.10, and applied contact force vector ${}_cf$

$${}_s\tau = \vec{r} \times_c f \in \mathbb{R}^{3\times1} \tag{3.9}$$

The cross product in equation (3.9) can be written as the product between matrix R and force vector ${}_cf$

$${}_s\tau = R\ {}_cf = \begin{pmatrix} r_y \cdot_c f_z - r_z \cdot_c f_y \\ r_z \cdot_c f_x - r_x \cdot_c f_z \\ r_x \cdot_c f_y - r_y \cdot_c f_x \end{pmatrix} \in \mathbb{R}^{3\times1} \tag{3.10}$$

yielding the skew-symmetric matrix R, defined as

$$R = \begin{bmatrix} 0 & -r_z & r_y \\ r_z & 0 & -r_x \\ -r_y & r_x & 0 \end{bmatrix} \in \mathbb{R}^{3\times 3} \tag{3.11}$$

It is interesting too look at (3.5), which shows that the contact point can be retrieved in the absence of a contact torque and thus when a pure force is applied. In this case the equation would be as follows

$$\begin{bmatrix} 1 & 0 & 0 & 0 & 0 & 0 \\ 0 & 1 & 0 & 0 & 0 & 0 \\ 0 & 0 & 1 & 0 & 0 & 0 \\ 0 & -r_z & r_y & 1 & 0 & 0 \\ r_z & 0 & -r_x & 0 & 1 & 0 \\ -r_y & r_x & 0 & 0 & 0 & 1 \end{bmatrix} \begin{pmatrix} {}_sf_x \\ {}_sf_y \\ {}_sf_z \\ {}_s\tau_x \\ {}_s\tau_y \\ {}_s\tau_z \end{pmatrix} = \begin{pmatrix} {}_cf_x \\ {}_cf_y \\ {}_cf_z \\ 0 \\ 0 \\ 0 \end{pmatrix} \tag{3.12}$$

which shows that in the absence of contact torques ${}_c\tau$, the components of the position vector $\vec{r}$ can be retrieved. This feature is currently not used but might be useful for future applications. Another feature that might be useful, is the ability of the force plate to determine contact torques, this however is only possible in certain cases. When a contact force and contact torque are applied to the force plate at the same time, the point of contact must be known in order to be able to determine what the exact contact torque is. This is the case due to the fact that the contact forces will apply an additional torque to the sensor. This contact point cannot always be determined with purely the data of the force torque sensor, which implies the need of an external sensing method to obtain the contact point in case it is desired to measure the contact torques for all cases.

3.2.4 Measurement errors in the force plate

Error due to plate deflection

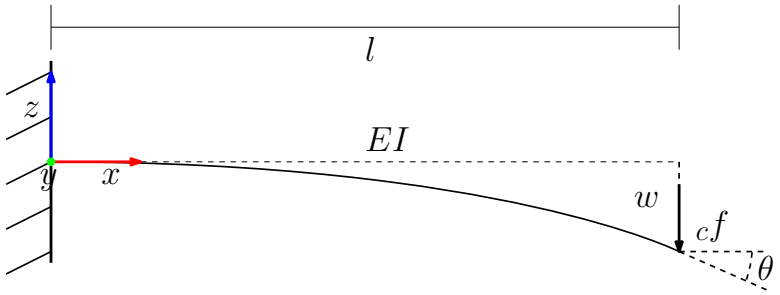

Figure 3.11: Vertical load case causing plate deflection

In order to determine errors due to deflection, the direction with the lowest stiffness is considered which is the z-direction as indicated in figure 3.11. Modeling one half of the plate as a clamped beam at one end with its length equal to half the length of the total plate $l = 0.5L$, the deflection and deflection angle due to an external load ${}_cf$ can be determined according to [7] as follows

$$w = \frac{{}_cfl^3}{3EI} \tag{3.13}$$

$$\theta = \frac{{}_cfl^2}{2EI} \tag{3.14}$$

With w the deflection and θ the deflection angle. The parameter I represents the area moment of inertia and can be computed with respect to an axis which is collinear with the base as

$$I = \frac{Wh^3}{3} \tag{3.15}$$

for a rectangle with dimensions $W \times h$. Parameter E represents the young's modulus of the plate and is thus dependent on the used material.

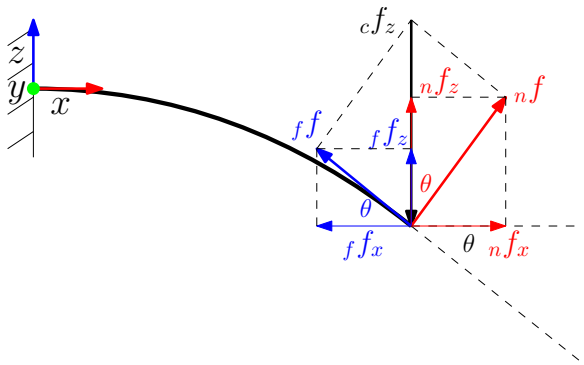

Figure 3.12: Reaction forces

Figure 3.12 shows that in the case of sufficient surface friction of the plate, the contact force can be sensed completely causing no measurement error. This is the case because the deflection of the plate itself doesn't cause a rotation of the sensor frame. It is however desired to have as little deflection as possible as it is stated in the manual of the force torque sensor that low plate deflections on the contact surface between sensor and tool, will result in the highest accuracy.

Error due to sensor stiffness

To determine the error due to the stiffness of the sensor, first the stiffness in $x-$ and $y-$direction must be considered, which is listed in table 3.1 as $K_{Txy} = 1.1{\cdot}10^4$ [Nm/rad]. Due to the placement and stiffness of the sensor the tool adapter plate will rotate which is depicted in figure 3.6. This causes the sensor frame to rotate as well causing inaccuracies in the measurements.
To give an indication about the measurement error due to the sensor stiffness it is assumed that a vertical load of 10 N is applied at the edge of the plate. This results in an applied moment of $T_y =_c f_z \times l = 10 \times 0.15 = 1.5$ [Nm] causing a rotation of $\phi = \frac{T_y}{K_{txy}} = \frac{1.5}{1.1{\cdot}10^4} = 1.4 \cdot 10^{-4}$ [rad].

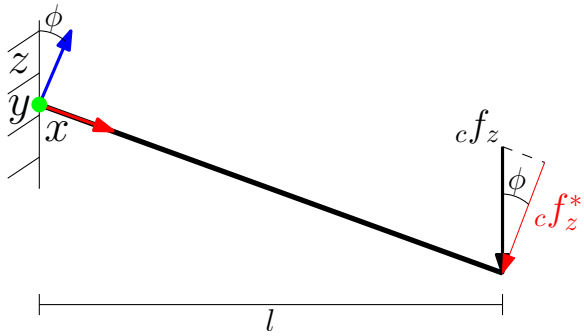

Figure 3.13: Deflection due to sensor stiffness

Figure 3.13 shows that the rotation of the sensor frame causes measurement errors. Due to this deflection, an applied load of 10 N at the edge of the plate is being sensed as a smaller load which can be computed as

$$ {}_c f_z^* =_c f_z \cdot \cos\phi \tag{3.16}$$

Due to the extremely small deflection because of the sensor stiffness, it will have a very small effect on the accuracy. Substituting the rotation of $1.4 \cdot 10^{-4}$ of this specific load case into (3.16) will therefore result in the measured force in z-direction approximately being equal to the real force in z-direction and thus ${}_c f_z^* \approx_c f_z$.

3.2.5 Calibration of the force plate

In order to ensure the force plate measures the contact forces correctly and to give a first order indication of its accuracy, a calibration procedure needs to be performed for all degrees of freedom. Although a full calibration in all the degrees of freedom has not been executed and still has to be performed, a partial calibration has been done for forces in the z-direction. During this calibration, several observations regarding the measurements are done which will be listed at the end.
Figure 3.14 shows the calibration setup in which the force plate is clamped to the table. To calibrate the force plate for forces in the z-direction the top plate has been divided into a grid of 9 positions with distances of 10 cm in between. A schematic figure of this grid is shown in figure 3.15. By placing weights with varying mass on these 9 positions it can be observed if the force plate registers the applied forces correctly. It can be observed as well if the force plate makes errors in measuring the contact forces and if this is the case it can be observed how large these errors are.

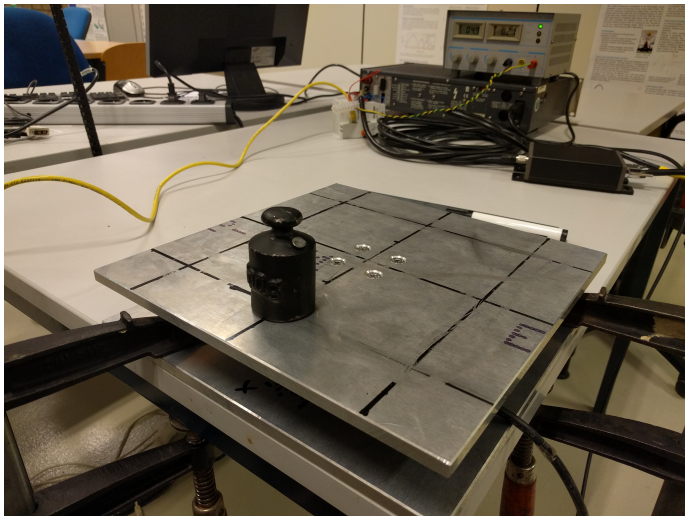

Figure 3.14: Force plate calibration setup

First, the signals are observed in the case of no external load applied on the force plate. Ideally the resulting signal would thus be equal to zero for all degrees of freedom. This is not the case however, since the sensor shows an offset which we will define as the bias error $\vec{E_b}$. This bias error is a vector with dimensions 6×1, containing the biases in the force and torque for each degree of freedom. To determine the bias of the force plate, the output signal of the sensor is captured for 8 seconds with a frequency of 100 Hz, after which it is averaged over time. The bias error has to be subtracted from the sensor signal, to obtain a signal equal to zero for all degrees of freedom. Typical values for the bias error of this force plate are equal to

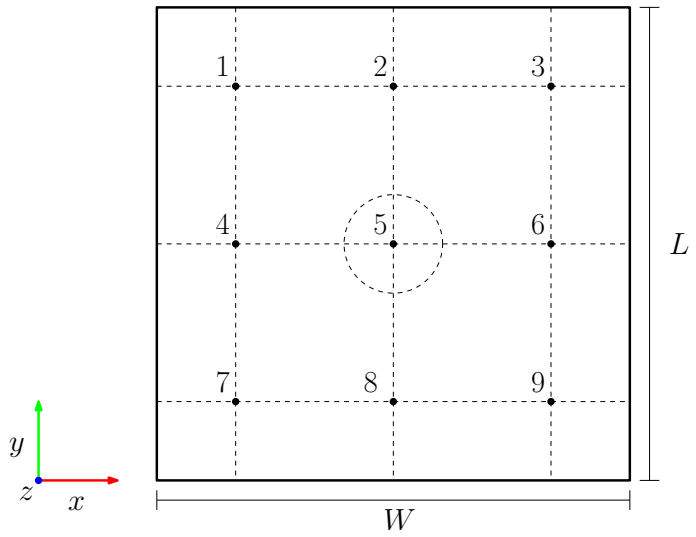

Figure 3.15: Force plate calibration positions

$$\vec{E_b} = \begin{pmatrix} E_b^x \\ E_b^y \\ E_b^z \\ E_b^{tx} \\ E_b^{ty} \\ E_b^{ty} \end{pmatrix} = \begin{pmatrix} -0.0679 \\ -1.2069 \\ -28.3432 \\ -0.3026 \\ -0.0295 \\ -0.0855 \end{pmatrix} \begin{matrix} [\text{N}] \\ [\text{N}] \\ [\text{N}] \\ [\text{Nm}] \\ [\text{Nm}] \\ [\text{Nm}] \end{matrix}$$

in which the large bias error in the z-direction can be noticed, which is due to the weight of the top plate. This weight has therefore be compensated. It has also been observed that the bias error slightly changes over time. This could be caused by variations of the environment parameters as the temperature. For most accurate results the bias factor is therefore determined shortly before the actual measurement.
To determine the measurement errors that occur while applying forces in the z-direction, 3 different weights are placed at the 9 grid positions shown in figure 3.15. Each measurement takes a total of 20 seconds of which the first time interval $t = 0 - 8$ s is used to determine the bias error. The second time interval $t = 8 - 12$ s is used for any vibrations that have been caused by placing the weight to damp out. Finally, time interval $t = 12 - 20$ s is used to determine the error which is defined as the mean absolute error

$$E_m = \frac{1}{n} \sum_{t=12}^{t=20} |e(t)| \tag{3.17}$$

with n the number of measurements and $e(t)$ the error between the measured force and the actual force at time t.
The first weight that has been used for calibration has a mass of $m_1 = 0.0135$ kg which results in a force of $F_1 = 0.1324$ N when placed on the force plate. The second weight has a mass of $m_2 = 0.4998$ kg which corresponds to a force of $F_2 = 4.9030$ N which is roughly half of the maximum payload of the ULNA arm. The mass of the third weight is $m_3 = 2.005$ kg corresponding to a force of $F_3 = 19.669$ N or roughly twice the maximum payload of the ULNA arm. The mass of all weights is measured beforehand on a scale for maximum accuracy.

Tables 3.3, 3.4 and 3.5 show the mean average error in ${}_cf_x$, ${}_cf_y$ and ${}_cf_z$ over time interval $t = 12-20$ s of the measurements in 9 grid positions. This is done for all 3 loads F_1, F_2 and F_3. The measurements are corrected with the bias error which is determined in time interval $t = 0 - 8$ s.

It can be observed that the error in ${}_cf_z$ is small and remains within the specified accuracy of 0.1 N which is defined in table 3.2. The error in this degree of freedom remains small even though the magnitude of the force is increased.
Another thing that can be observed is that while the ${}_cf_z$ remains more or less the same, the error in ${}_cf_x$ and ${}_cf_y$ increases while the load is increased. It can also be seen that the magnitude of this error is different for every position the load is applied. Since there is no load applied in x- and y-direction it is interesting to see that the force plate does register a force in these directions and that these registered forces are increasing when increasing the load in z-direction. A possible explanation for this effect could be that the sensor needs recalibration. The manufacturer recommends annual recalibration while the latest calibration of this sensor is 3 years ago. Unfortunately this can only be done in the manufacturers lab.

Position	**1**	**2**	**3**	**4**	**5**	**6**	**7**	**8**	**9**
${}_cf_x$	0.0103	0.0112	0.0155	0.0216	0.0599	0.0306	0.0294	0.0116	0.0210
${}_cf_y$	0.0087	0.0100	0.0152	0.0200	0.0416	0.0116	0.0079	0.0254	0.0275
${}_cf_z$	0.0167	0.0282	0.0295	0.0240	0.0189	0.0405	0.0412	0.0395	0.0276

Table 3.3: Errors in ${}_cf_x$, ${}_cf_y$ and ${}_cf_z$ for an applied load of $F = 0.1324$ N in z-direction for all 9 grid positions

Position	**1**	**2**	**3**	**4**	**5**	**6**	**7**	**8**	**9**
${}_cf_x$	0.1035	0.0261	0.0245	0.0667	0.0154	0.0716	0.0147	0.0769	0.1474
${}_cf_y$	0.1054	0.1136	0.0959	0.0246	0.0111	0.0119	0.0769	0.0959	0.1230
${}_cf_z$	0.0175	0.0210	0.0179	0.0210	0.0180	0.0214	0.0254	0.0195	0.0180

Table 3.4: Errors in ${}_cf_x$, ${}_cf_y$ and ${}_cf_z$ for an applied load of $F = 4.9030$ N in z-direction for all 9 grid positions

Position	**1**	**2**	**3**	**4**	**5**	**6**	**7**	**8**	**9**
${}_cf_x$	0.3655	0.1422	0.0947	0.1567	0.0736	0.2957	0.0296	0.2416	0.4543
${}_cf_y$	0.3295	0.3824	0.3484	0.0514	0.0294	0.0344	0.3677	0.3792	0.3717
${}_cf_z$	0.0591	0.0195	0.0617	0.0275	0.0411	0.0194	0.0683	0.0475	0.0316

Table 3.5: Errors in ${}_cf_x$, ${}_cf_y$ and ${}_cf_z$ for an applied load of $F = 19.669$ N in z-direction for all 9 grid positions

For the purpose of showing typical results obtained by using the force plate, several measurements recording tasks that could be performed in real life are presented in Appendix B. These tasks include a straight line wiping motion with a plastic object, a circular wiping motion and writing text on paper.

3.3 Summary

This chapter addressed the simulation environment that is designed as a tool to study the sensitivity of the residual method to parameter uncertainty and addressed the following important points.

- The simulator is able to visualize the motion of the 7 DOF ULNA arm and shows its contact with the environment which is defined as a flat and static surface, with the task specification defined as the arm wiping over the surface in the plane parallel to the surface, while maintaining a desired force in the direction normal to the surface.
- The friction of the surface is modeled as a combination of Coulomb and viscous friction while the Hunt-Crossley model is implemented for modeling the normal forces to ensure a smooth transition when the end effector comes in contact with the surface.
- The residual equation is modified to include friction in the joints to study its effect on the estimation. The joint friction is modeled as a combination of Coulomb and viscous friction.
- Computation of the reference trajectory is done with the Jacobian inverse technique to obtain desired joint trajectories from the desired end effector trajectory.
- A force plate has been realized using a 6 DOF force torque sensor, that is able to measure contact forces. An initial calibration procedure is executed for measuring the contact forces in the z-direction. The calibration of the measurements of contact forces in the x- and y-directions still needs to be done.

Chapter 4

Sensitivity analysis of the residual method

This chapters describes the findings of the sensitivity analysis of the residual method to parameter uncertainty. First, the trajectory of the end-effector will be addressed after which the results and effect of introducing uncertainty in the Coulomb friction parameters on the estimation of the contact force will be covered. We will compare the estimated contact force with the true contact force for both the ideal case and the case in which uncertainties are introduced in the Coulomb friction.

4.1 End effector trajectory

The two end effector trajectories that will be used for the simulations can be seen in Figure 4.1, in which the trajectory in the x, y-plane is shown. The first plot shows a top view of the surface while the second and third plot show the trajectory in the x- and y- direction defined in the table frame R_T. The choice for this end effector trajectory is made because of the resemblance to a wiping motion. The robot will thus wipe the table in two different directions as indicated by the first subfigure of Figure 4.1.

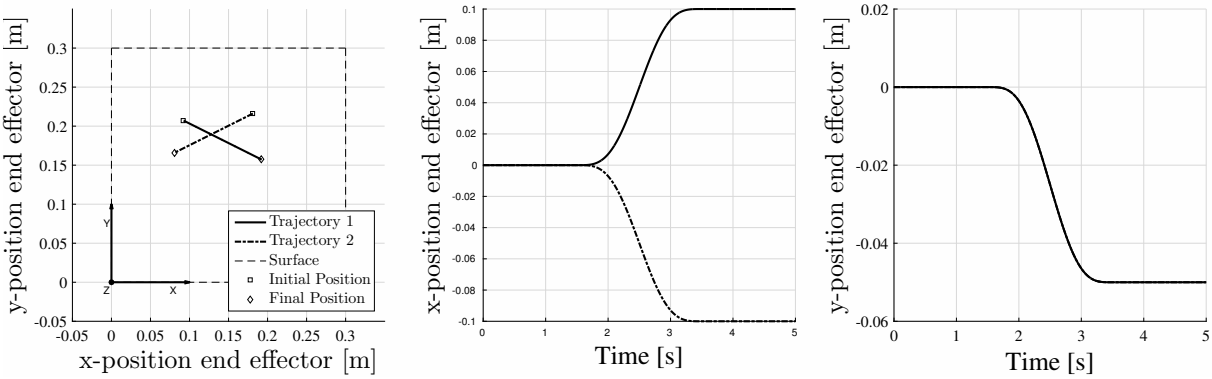

Figure 4.1: End effector trajectory in x, y dimensions

The complete motion takes a total of 5 seconds to complete and can be divided in 5 parts as indicated in Figure 4.2, in which the trajectories in z-direction are shown. The robot starts with its end effector at a fixed distance above the surface. In part 1 of the trajectory, the end effector descends towards the table until it is at the exact height as the table, and in which still no contact force is exerted on the end effector. In part 2 of the trajectory, the end effector penetrates the

surface until it reaches the desired contact force F_z^d. Part 3 of the trajectory involves the end effector wiping over the surface while maintaining a desired contact force F_z^d in the direction normal to the surface. In part 4 of the trajectory the end effector is exiting the surface until it is at equal height of the surface, which again leads no contact force being exerted on the end effector anymore. In part 5 the end effector is raised from the table and stopped at a fixed height.

Figure 4.3 shows the 2nd and 4th part of the first trajectory in more detail in which it is important to notice the scale of the y-axis. As stated above, the end effector penetrates the surface in between t = 1-1.5, and exits the surface in between t = 3.5-4. The penetration of the table is needed to set a desired normal force F_z^d, which can be computed by taking the first term in (3.1)

$$F_n(t) = kx_p(t)^\alpha \tag{4.1}$$

representing the elastic term, and by rewriting it as

$$x_p(t) = \left(\frac{F_n(t)}{k}\right)^{\frac{1}{\alpha}} \tag{4.2}$$

to obtain the desired penetration $x_p(t)$ needed for a desired normal force.

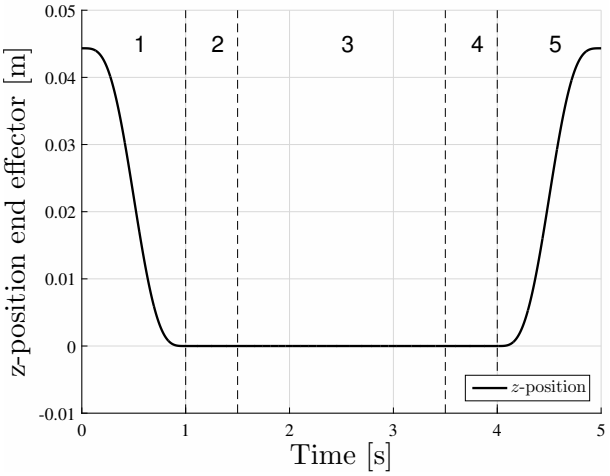

Figure 4.2: The trajectory in z direction, divided in 5 parts

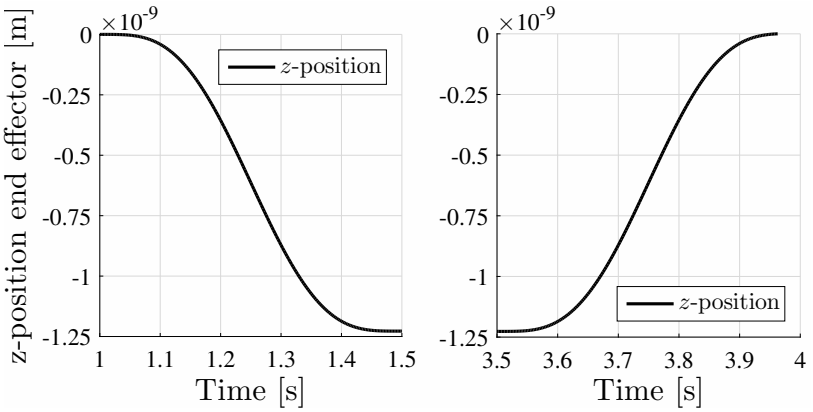

Figure 4.3: Trajectory in z direction in time intervals t = 1-1.5 and t = 3.5-4

Figures 4.4, 4.5 and 4.6 show the normalized joint position, velocity and acceleration trajectories for all 7 joints corresponding to the first desired cartesian end effector trajectory of figure 4.1. It can be observed that the iterative inverse kinematics solution described in section 3.1.5 produces smooth joint trajectories.

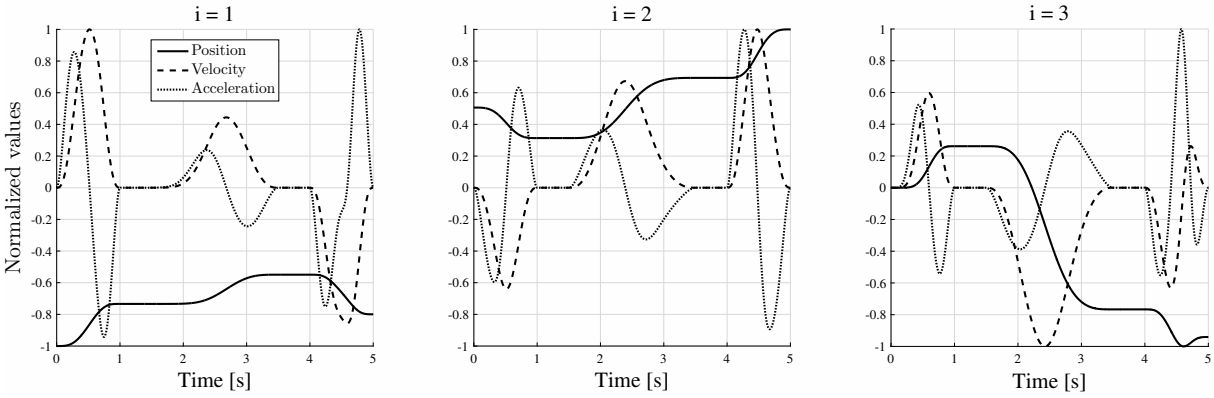

Figure 4.4: Joint trajectories of joints 1, 2 and 3

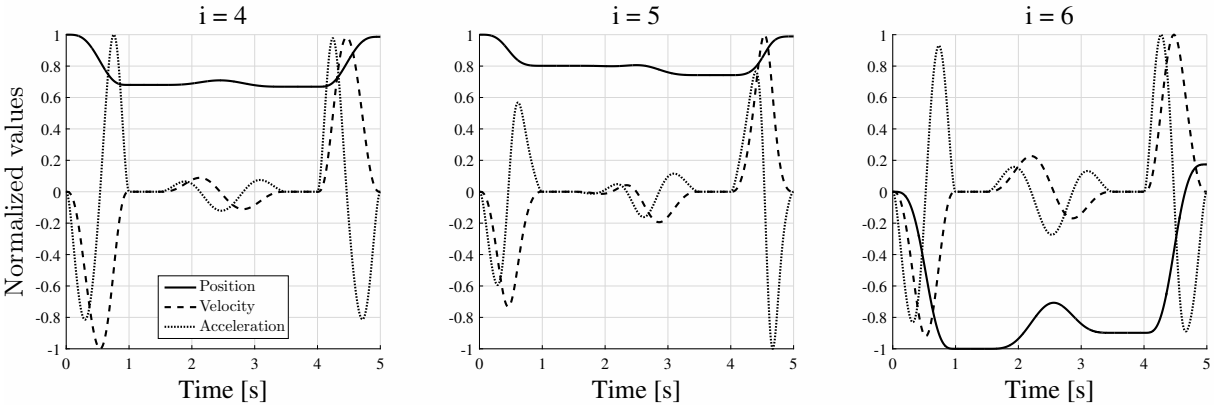

Figure 4.5: Joint trajectories of joints 4, 5 and 6

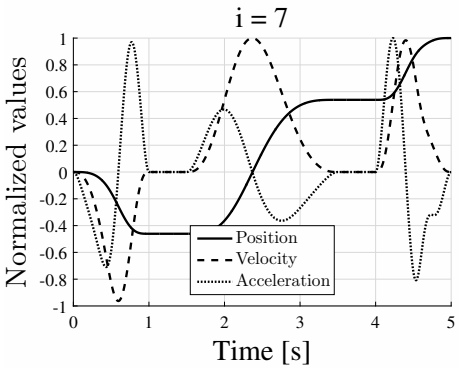

Figure 4.6: Joint trajectory of joint 7

4.2 Sensitivity with respect to uncertainty in the Coulomb friction

In this subsection the results of the sensitivity to parameter uncertainty in the Coulomb friction for the estimated contact force are presented. First, the ideal case will be presented to show that the estimation algorithm works as expected. Hereafter, parameter uncertainties are introduced in the Coulomb friction to examine its effect on the contact force estimation.

4.2.1 Contact force estimation in ideal circumstances

To determine if the contact force estimator performs as desired, it is assumed in this first test case that complete information is known about the dynamic model of the robot. In the case of a well performing estimator it is expected to be able to estimate the contact force with a minimal error since there is absolutely no parameter uncertainty. Figure 4.7, 4.8 and 4.9 show the results of the estimation of the residual vector $\mathbf{r(t)}$ plotted against the true torque vector τ_e exerted by the environment on the robot, for all 7 joints. Due to the fact that the difference between the external torque and the residual is almost not visible in these figures, the errors are quantified in tables 4.1 and 4.2. It is still interesting however, to observe the profiles of the external applied torque τ_e. Notice the jumps in the torque at $t = 1.5$ s and $t = 3.5$ s. At these points in time, where there is a transition from zero to nonzero velocity or vice versa.

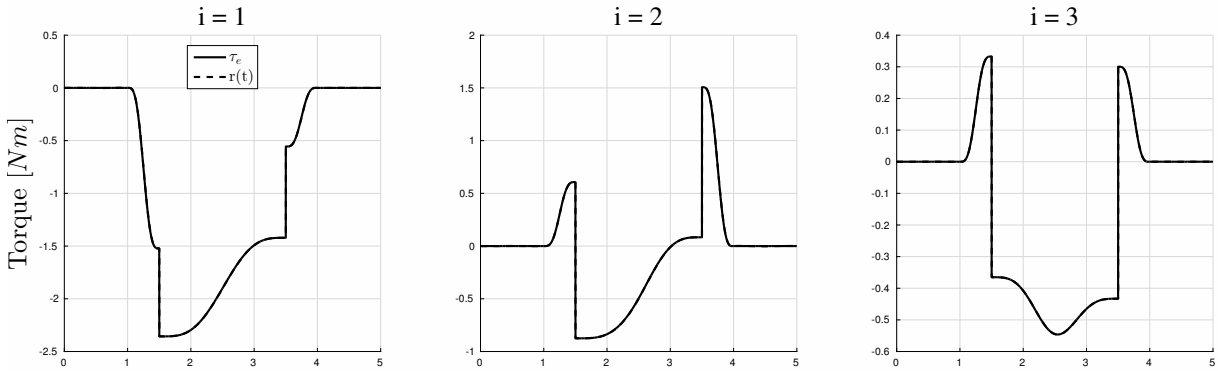

Figure 4.7: Estimated residual plotted against the true torque τ_e for joints i = {1, 2, 3} for no parameter uncertainty

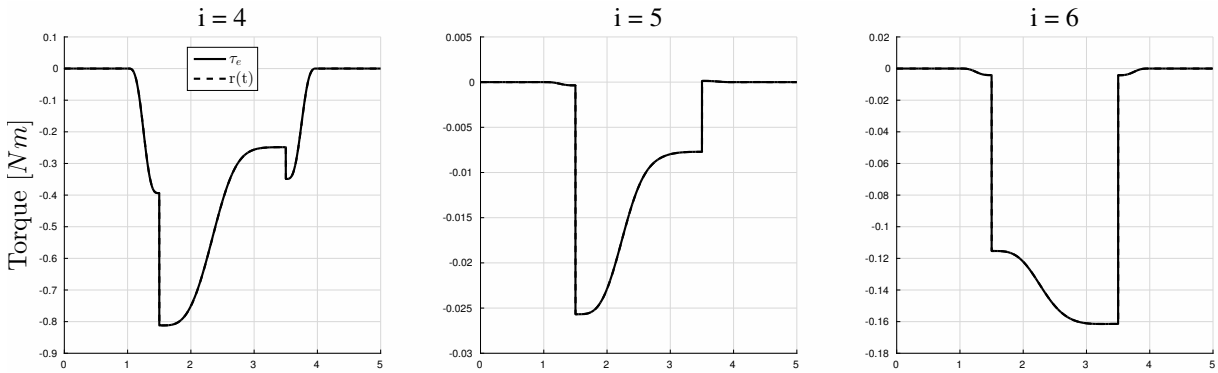

Figure 4.8: Estimated residual against the true torque τ_e for joints i = {4,5,6} for no parameter uncertainty

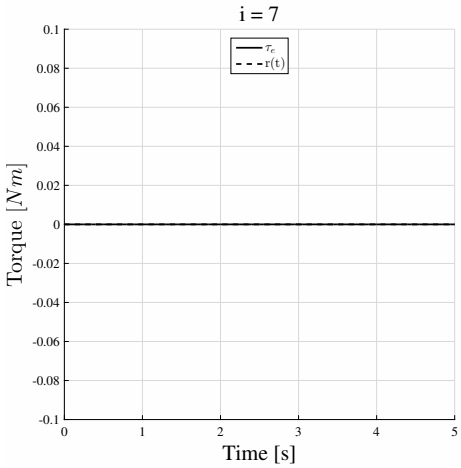

Figure 4.9: Estimated residual against true torque τ_e torque for joint i = 7 for no parameter uncertainty

Figure 4.10 shows the estimated contact forces $\hat{F}_x$, $\hat{F}_y$ and $\hat{F}_z$ plotted against the true contact forces in the case of no parameter uncertainty for trajectory 1, which again show that the estimator is able to estimate the contact force successfully. Observe again the jumps in F_x and F_y indicating a transition in velocity in the x- and y- direction while being in contact with the surface. Figure 4.11 shows plots of the errors in the force estimation. It can be seen that at time $t = 1.5$ and $t = 3.5$ a spike occurs in the error of the estimation of F_x and F_y due to the static friction of the surface.

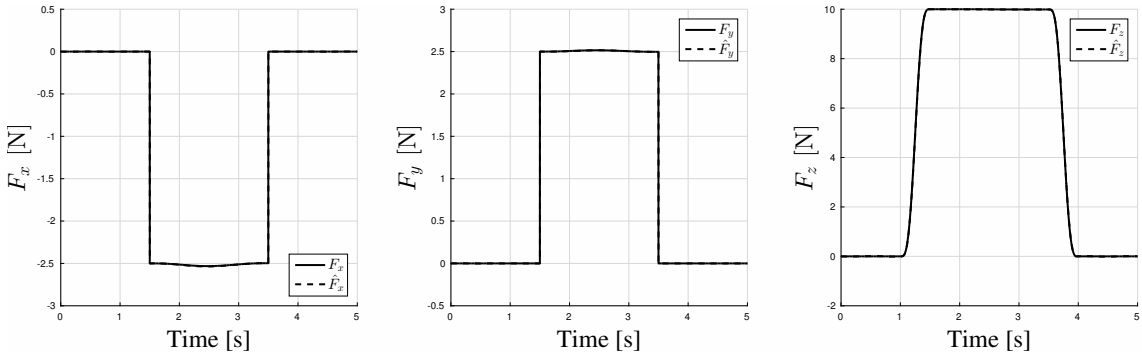

Figure 4.10: Estimated contact forces $\hat{F}_x$, $\hat{F}_y$ and $\hat{F}_z$ plotted against the true contact forces F_x, F_y and F_z in the case of no parameter uncertainty

In order to quantify the performance of the observer over time, the mean absolute error is computed according to [16] with the following equation

$$E_m = \frac{1}{n} \sum_{t=0}^{tF} |e(t)| \tag{4.3}$$

in which $e(t)$ represents the error of the estimation with respect to the true force at time t. The root mean square error is comuted as

$$E_{rms} = \sqrt{\frac{1}{n} \sum_{t=0}^{tF} e(t)^2} \tag{4.4}$$

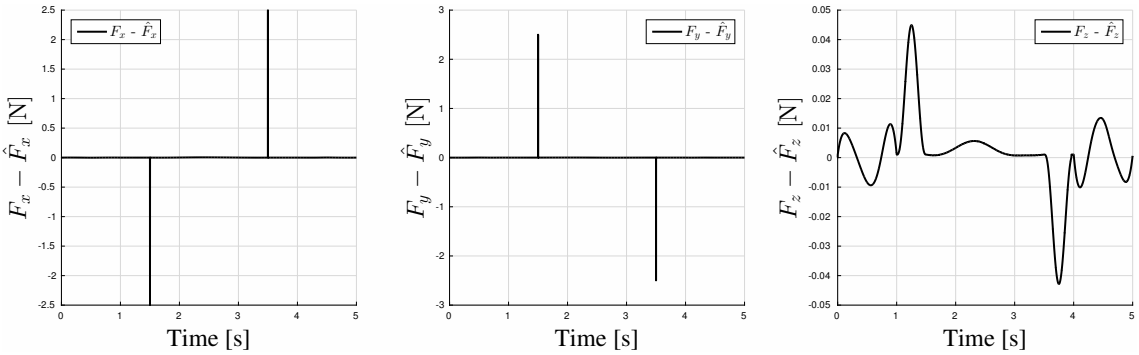

Figure 4.11: Error in $\hat{F}_c$ in the ideal case

Tables 4.1 and 4.2 show the mean absolute error E_{MAE} and the root mean square error E_{RMS} of the residual $\mathbf{r}(t)$ with respect to τ_e for all 7 joints and the mean absolute error of the estimated contact forces and moments $\hat{F}_c$ with respect to the true contact forces and moments F_c.

$\mathbf{r}_i$	E^1_{mae}	E^1_{rms}	E^2_{mae}	E^2_{rms}
1	0.0011	0.0171	0.0009	0.0192
2	0.0016	0.0291	0.0012	0.0164
3	0.0005	0.0143	0.0003	0.0091
4	0.0004	0.0061	0.0006	0.0170
5	0.0000	0.0004	0.0000	0.0003
6	0.0001	0.0027	0.0001	0.0025
7	0.0000	0.0000	0.0000	0.0000

Table 4.1: Mean absolute error E_{mae} and root mean square error E_{rms} for each of the 7 components of the residual vector $\mathbf{r}(t)$
for both trajectories

F_c	E^1_{mae}	E^1_{rms}	E^2_{mae}	E^2_{rms}
$\hat{F}_x$	0.0039	0.0502	0.0018	0.0500
$\hat{F}_y$	0.0023	0.0500	0.0015	0.0500
$\hat{F}_z$	0.0082	0.0128	0.0062	0.0118

Table 4.2: Mean absolute error E_{mae} and root mean square error E_{rms} for the estimatec contact force $\hat{F}_c$ for both trajectories

It can be observed even with exact knowledge of the parameters, there is still a small error present in the contact force estimation for both end effector trajectories. In appendix A.1 it is shown that varying the step size will have its effect on the accuracy of the estimation. The errors made in the ideal circumstances are small however and in the same order of magnitude for both trajectories.

4.2.2 Effects of uncertainty in the Coulomb friction coefficient

Estimation of the joint torques

To examine the effect of introducing uncertainty in the Coulomb friction parameters, we first introduce an uncertainty of ±10% in the Coulomb joint friction for all 7 joints at once. This is done by altering the Coulomb friction parameter for all joints in the parameters used in the residual method, to compare the results of the estimation to true values of the torque. The result is plotted in Figures 4.12, 4.13 and 4.14, in which the true external torque τ_e is plotted against the estimated residuals $r(t)$ for an uncertainty of 10 percent. The error is plotted below, which is the difference of the residual with respect to the true external torque.

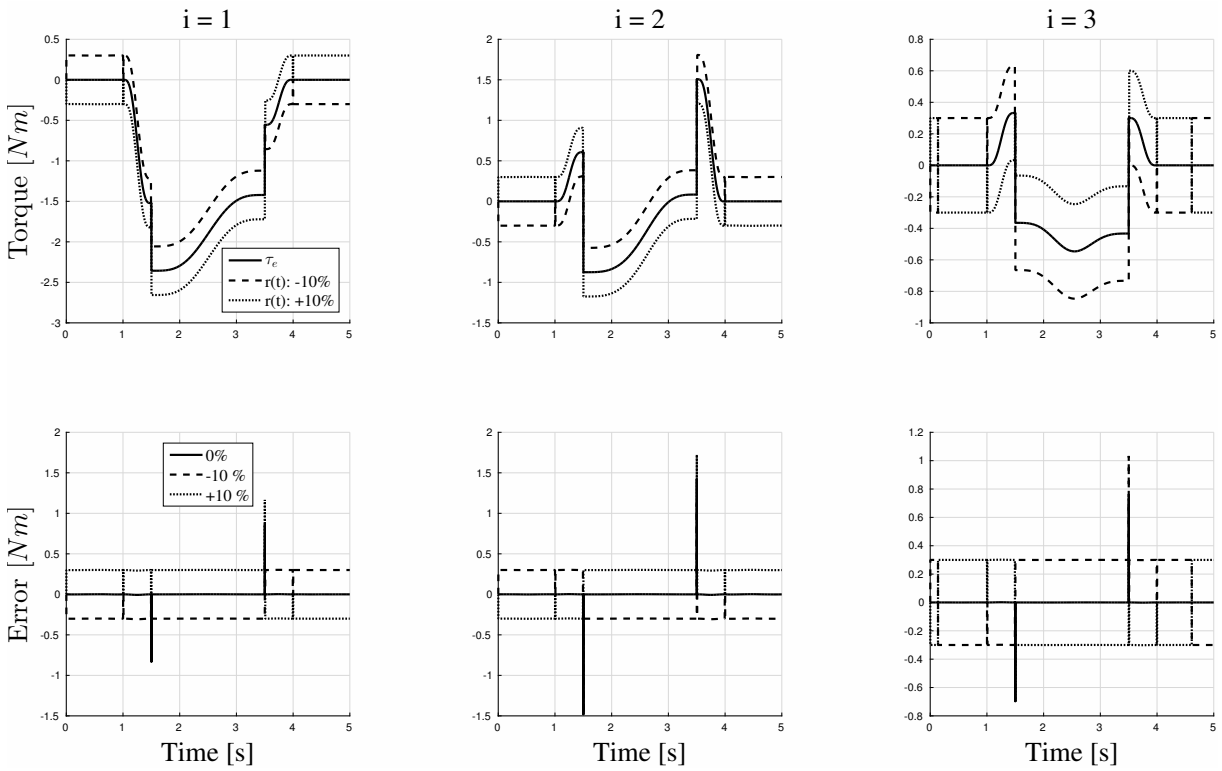

Figure 4.12: Error in $r(t)$ due to Coulomb friction for joints 1,2 and 3 with a 10 percent uncertainty

It can be seen that the residual method returns almost exactly the error that was introduced in the first place by introducing the uncertainty in the Coulomb friction coefficient by observing that the error of 0.3 Nm is equal the 10% of the Coulomb friction coefficient of $\mu_s = 3$. This shows that an error in the Coulomb friction model, can be translated directly in the error that the estimator makes when trying to estimate the joint torques with the residual $r(t)$.

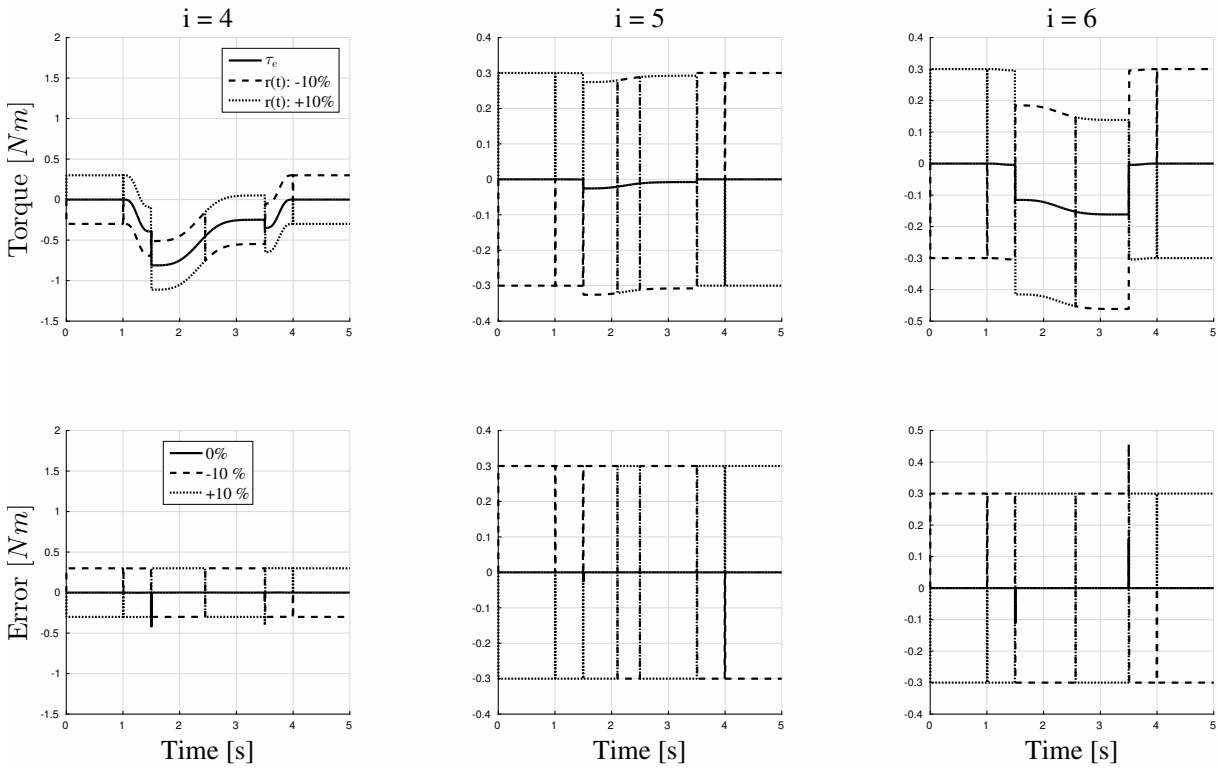

Figure 4.13: Error in $r(t)$ due to Coulomb friction for joints 4,5 and 6 with a 10 percent uncertainty

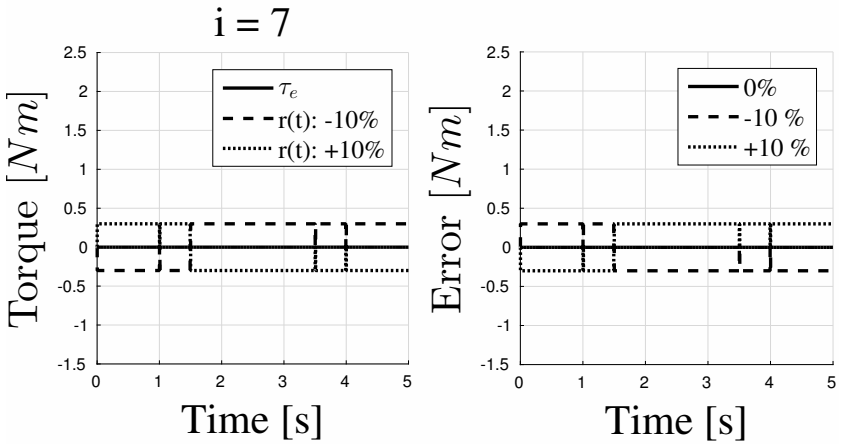

Figure 4.14: Error in $r(t)$ due to Coulomb friction for joint 7 with a 10 percent uncertainty

Estimation of the contact force

Figure 4.15 shows the results of estimating the contact force F_c in the case of an uncertainty in the Coulomb friction coefficient of $\pm 10\%$ corresponding to trajectory 1. The dashed lines in these Figures are indicated with either $+10\%$ or -10% depending on a positive or negative percentage uncertainty. The solid line indicates the true contact force. It can be observed that this results in a significant error in the estimation of the contact force $\hat{F}_c$ and that at certain intervals a force is detected in the case of no presence of a real external force. This can be seen when looking at the interval $t = 0 - 1$ s and $t = 4 - 5$ s. It can be observed too that although the overall error is significant, there are certain intervals in which the contact force estimation makes an error that approaches the true value more accurately. This can be observed for $\hat{F}_c^z$ in between $t = 2.5 - 3.5$ s.

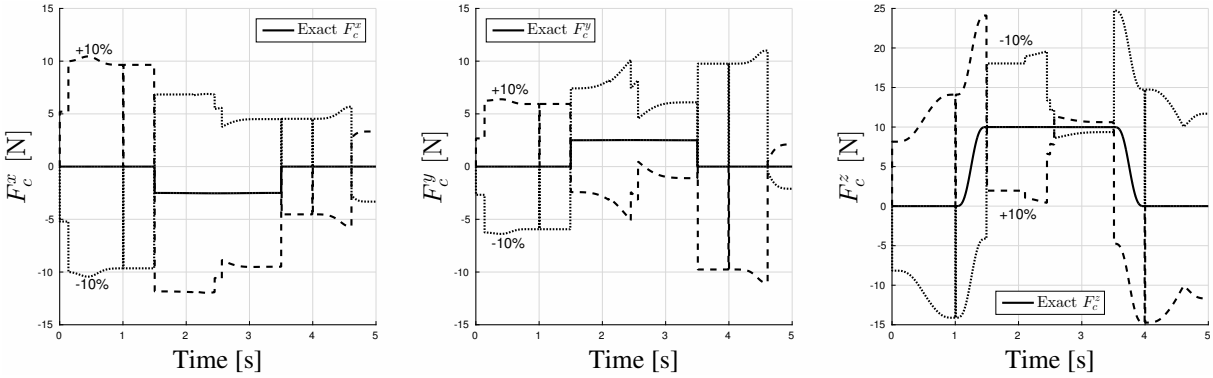

Figure 4.15: Estimated contact force $\hat{F}_c$ indicated by dashed lines for trajectory 1, showing the errors due to uncertainty in the Coulomb friction in all 7 joints

Figure 4.16 shows the results of estimating the contact force with an uncertainty of $\pm 10\%$ in the Coulomb friction parameter for trajectory 2. It can be observed that again a significant error is present in the estimation of the contact force. The magnitude of the error however is different in certain time intervals when compared to the contact force estimation for trajectory 1 in figure 4.15. This indicates that certain joint trajectories will affect the contact force estimation in such a way that better results are achieved for certain trajectories than for others.

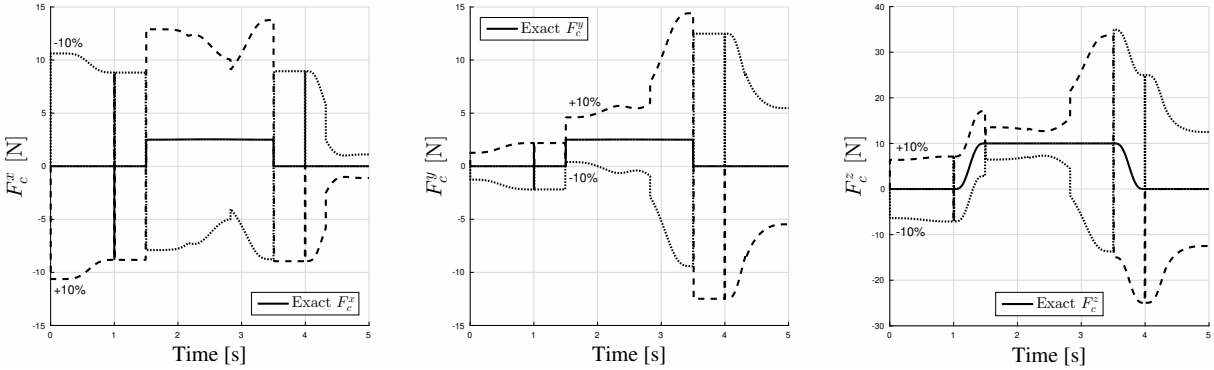

Figure 4.16: Estimated contact force $\hat{F}_c$ indicated by dashed lines for trajectory 2, showing the errors due to uncertainty in the Coulomb friction in all 7 joints

To examine the effect of the uncertainty in each joint separately, an uncertainty is introduced in the Coulomb friction parameter for each joint while not introducing an uncertainty for all other joints. The results for the contact force estimation are shown in Figures 4.17 and 4.18 for respectively trajectory 1 and 2. In these figures an uncertainty of a $\pm 10\%$ is introduced in the Coulomb joint friction parameter of joint 2, which is located in the shoulder of the arm. Similar results have been observed for the other joints making the choice to display the results for this joint arbitrary. It can be observed that the estimation remains within a reasonable limit of the true contact force and at some time intervals even results in a minimal almost zero error for $\hat{F}_c^y$ in trajectory 1 for $t = 1-2$ s.

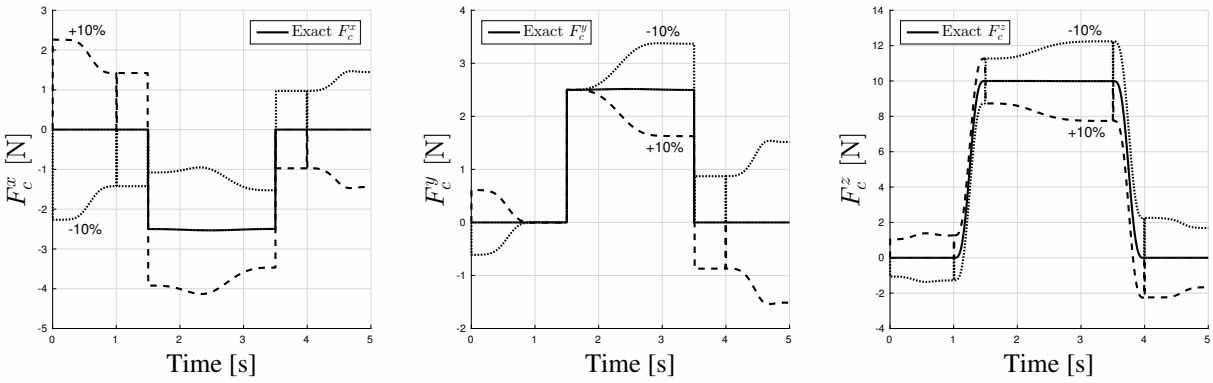

Figure 4.17: Estimated contact force $\hat{F}_c$ indicated by dashed lines, showing the errors due to uncertainty in the coulomb friction in joint 2 corresponding to trajectory 1

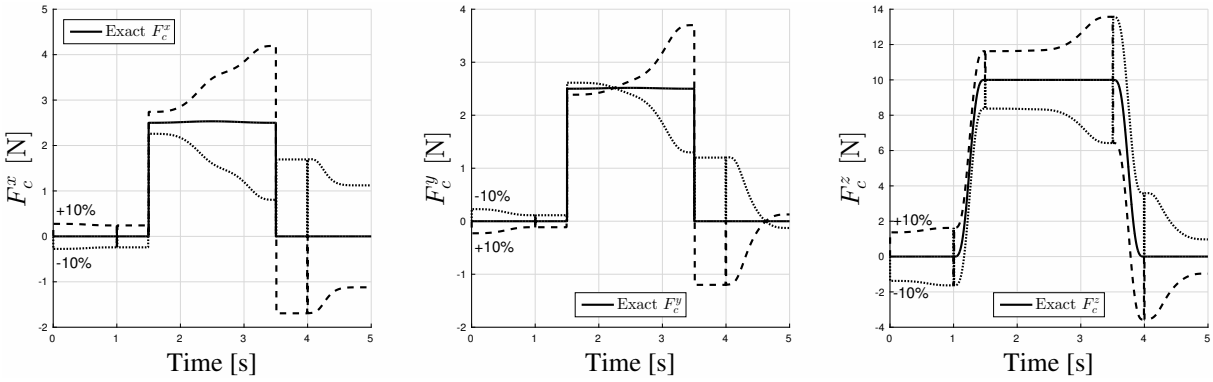

Figure 4.18: Estimated contact force $\hat{F}_c$ indicated by dashed lines, showing the errors due to uncertainty in the coulomb friction in joint 2 corresponding to trajectory 2

Sensitivity to Coulomb friction parameter uncertainty

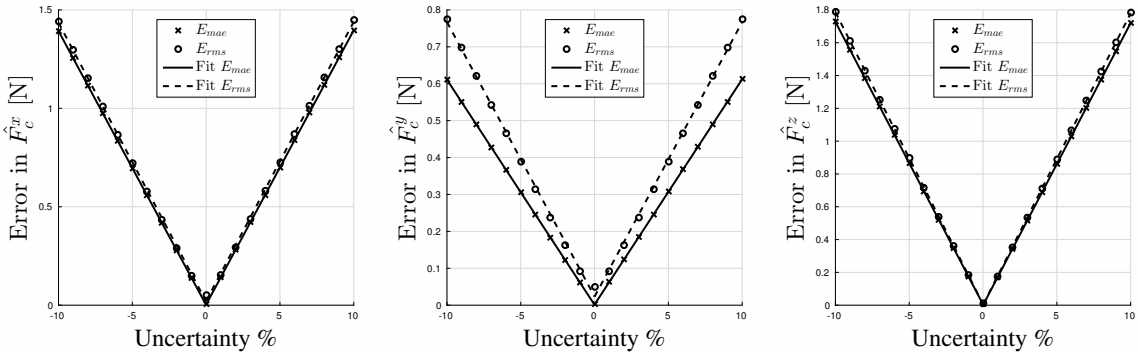

Figure 4.19: E_{mae} and E_{rms} in the estimated contact force $\hat{F}_c$ vs. parameter uncertainty in the joint friction for joint 2, trajectory 1

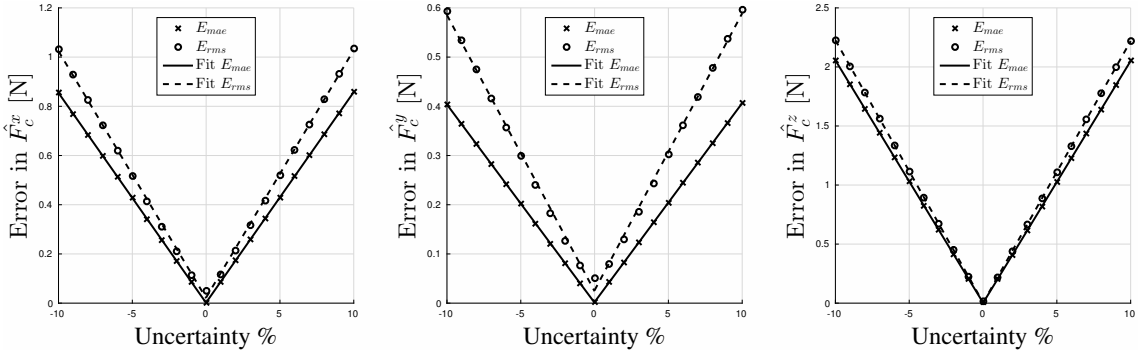

Figure 4.20: E_{mae} and E_{rms} in the estimated contact force $\hat{F}_c$ vs. parameter uncertainty in the joint friction for joint 2, trajectory 2

To analyze and quantify the error that is caused by the Coulomb friction parameter uncertainty, the mean absolute error and root mean square error are computed as presented in (4.3) and (4.4) respectively. This is done in a range from -10% to $+10\%$ with a resolution of 1% for both trajectories, while only introducing uncertainties in a single joint at a time. This thus results in a total of $7 \cdot 21 = 147$ simulations for each trajectory.
Figures 4.19 and 4.20 show the mean absolute error E_{mae} and the root mean square error E_{rms} in the estimated contact force for trajectory 1 and 2 respectively. These values are plotted against percentage parameter uncertainty in the Coulomb friction. When observing the plotted data points it can be seen that these error increases linearly with the uncertainty in the Coulomb friction for all contact force directions x, y and z, but that they have a different slope. This slope is defined as the sensitivity S, and is determined by a linear fit through the data points of E_{mae} and E_{rms}. The higher the sensitivity, the more sensitive the contact force estimation is towards errors in the corresponding joint. When looking at the sensitivities for the other joints it can be concluded that they are all linear in nature, looking similar to Figures 4.19 and 4.20, but with a different slope. This means that the contact force estimation differs in sensitivity for each joint. The sensitivity S is computed to determine magnitude of the sensitivity for each joint and for both trajectories. The magnitude of the sensitivity quantifies the error per percentage of uncertainty in the Coulomb joint friction. This way it can be shown which joint contributes the most towards the error in the contact force estimation.

Figure 4.21 and 4.22 show plots of the sensitivity S_{mae} and S_{rms} for each joint in the three cartesian directions, for trajectory 1 and 2 respectively, thus showing the joints that contribute the most to the overall error in the contact force estimation $\hat{F}_c$.

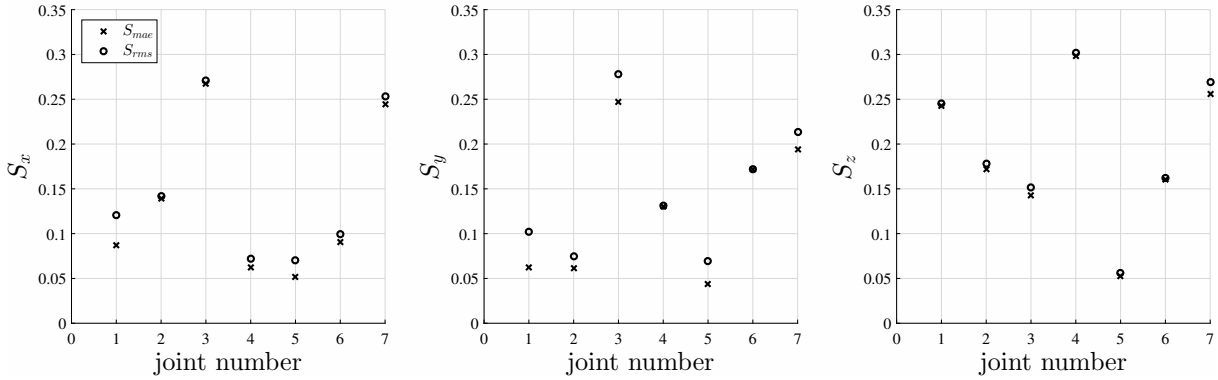

Figure 4.21: Magnitude of the Sensitivity S of each joint, for contact force estimation in direction x, y and z for trajectory 1

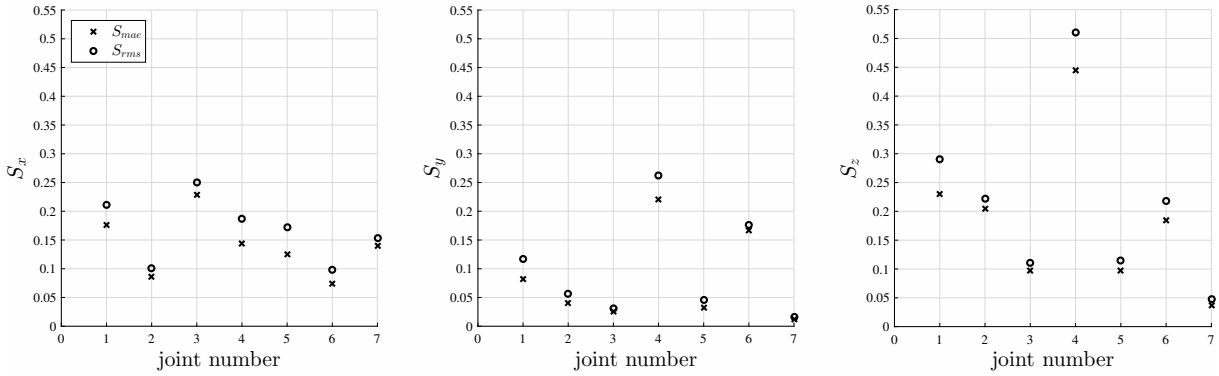

Figure 4.22: Magnitude of the Sensitivity S of each joint, for contact force estimation in direction x, y and z for trajectory 2

It can be observed that different results are obtained for the two trajectories while looking at the magnitudes of the sensitivities for each joint. When observing the results for trajectory 1 in figure 4.21, it can be seen that observed that the maximum value for the sensitivity lies around $S \approx 0.3$, and is obtained for S_x and S_y for joint 3. The maximum value for S_z can be observed for joint 4. When observing the results for trajectory 2 in figure 4.22, it can be seen that different values are obtained for the sensitivity compared to the results for trajectory 1. For S_x it can be seen that the the maximum sensitivity for joint 3 has slightly decreased to $S_x \approx 0.25$. It can be seen as well that for S_y the maximum sensitivity is now reached for joint 4 instead of joint 3 for trajectory 1 and is around equal in value. Perhaps the most interesting observation can be done when comparing values for S_z for trajectory 1 and 2. It can be seen that the maximum sensitivity for S_z is reached for joint 4, but that its magnitude for trajectory 2 is $S_z \approx 0.5$ and thus significantly higher.
The differences in sensitivities indicate that the force estimation method is less sensitive towards parameter uncertainty in the Coulomb friction for one trajectory than it is when the robot moves with another trajectory. By altering the joint trajectory, the sensitivity for parameter uncertainty can thus be altered as well. Furthermore, it can be observed as well that S_{mae} and S_{rms} are not equal in magnitude in all cases indicating a bigger contribution of large errors since these large errors are weighed more when computing the root mean squared error E_{rms}.

Ideally it would be desirable to compute what accuracy in determining the parameter uncertainty for the Coulomb friction would be required to still obtain a contact force estimation that is usable. Although it is hard to define this, we introduce a threshold of 10 percent in the error between contact force estimation $\hat{F}_c$ and true contact force F_c as a rule of thumb. This means that if the average error of the contact force estimation over time stays below 10 percent, it is considered a usable result.

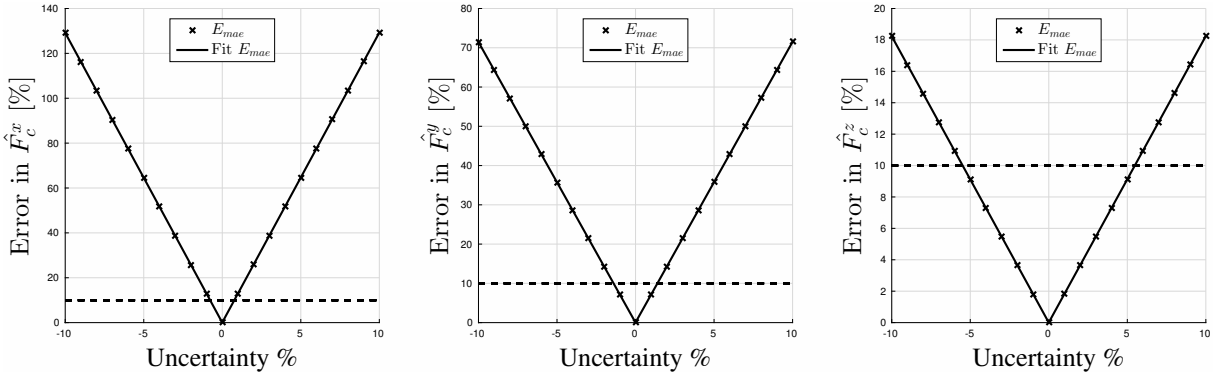

Figure 4.23: Uncertainty in the Coulomb friction parameters for all 7 joints vs. the mean average percentage error E_{mape} in time interval $t = 1.5 - 3.5$ s, for trajectory 1

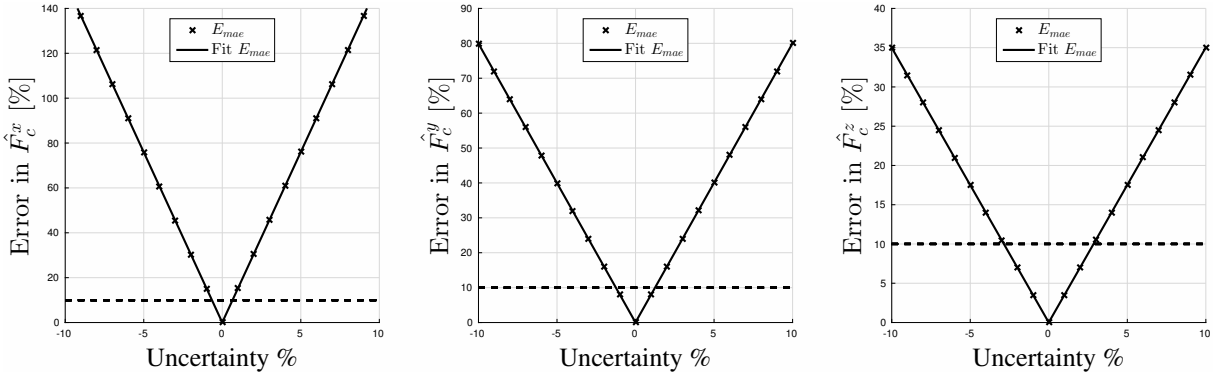

Figure 4.24: Uncertainty in the Coulomb friction parameters for all 7 joints vs. the mean average percentage error E_{mape} in time interval $t = 1.5 - 3.5$ s, for trajectory 2

To determine what percentage uncertainty in the Coulomb friction parameter leads to usable results, uncertainties are introduced for all 7 joints ranging from -10% to $+10\%$. The mean absolute percentage error is then computed as

$$E_{mape} = \frac{100}{n} \sum_{t=0}^{tF} \left| \frac{e(t)}{F_c(t)} \right| \tag{4.5}$$

in which $e(t)$ is the difference between the actual and estimated contact force at time t, and $F_c(t)$ the actual contact force at time t. The downside of this error quantification is that it is only possible to compute the error when there is an actual contact force. A contact force equal to zero would lead to an infinite value due to the denominator in (4.5). Because of this limitation the mean absolute percentage error E_{mape} is only computed for the time interval $t = 1.5 - 3.5$ s, for which it is known for sure that external contact forces are exerted on the robot. This error is then plotted against the uncertainty in the Coulomb friction parameter for all 7 joints of which the results can be seen in Figures 4.23 and 4.24.

These plots show that an uncertainty of approximately 1% in the Coulomb friction coefficient for all 7 joints leads to an error E_{mape} of 10 percent for the contact force estimations $\hat{F}_c^x$ and $\hat{F}_c^y$. This is the case for both trajectories and when the robot is in the contact phase.
The contact force estimation in the z-direction shows a different result where an uncertainty of approximately 5% in the Coulomb friction parameter results in an error E_{mape} of 10 percent for the contact force estimation of $\hat{F}_c^z$ for trajectory 1. An uncertainty of approximately 3% in the Coulomb friction parameter, results in an error E_{mape} of 10 percent in $\hat{F}_c^z$ for trajectory 2.

4.3 Summary

In this chapter we studied the sensitivity of the residual method to parameter uncertainty in the Coulomb friction, in which the following important points are addressed.

- In order to study the sensitivity of the residual method to parameter uncertainty, two end effector trajectories are considered. Both of these trajectories can be described as a wiping motion in a straight line. First the end effector moves in the direction normal to the table after which it starts pressing with a constant force. The wiping motion in a straight line is then initiated, all while the constant force in the normal direction of the table is maintained. At the end of the straight line, when the wiping motion is over, the end effector is again lifted up above the surface.

- To determine if the residual method works as intended, a study for ideal circumstances is conducted. This study shows that errors are minimal and appear to be numerical which is shown in Appendix A.

- An uncertainty of $\pm 10\%$ is introduced in the Coulomb friction coefficient for all joints. This shows that the error in the Coulomb friction model can be translated directly in the error the residual method makes when estimating the joint torques by computing $r(t)$.

- It is shown that an uncertainty of $\pm 10\%$ in the Coulomb friction coefficient in all joints leads to significant errors in the estimation of the contact force $\hat{F}_c$. It is also shown that the magnitude of the error in the estimation is different per trajectory. In certain time intervals the error in the estimation is much smaller than in other time intervals. The same can be observed when an uncertainty is introduced in only 1 joint.

- To study the sensitivity, the mean absolute error and root mean square error are computed over the complete time interval $t = 0{-}5$ s for both trajectories. This is done while introducing an uncertainty in only a single joint at a time. The magnitude of this uncertainty is done in the range of -10% to 10% to see how the error varies with changing uncertainty. It can be seen that the errors in the estimation of the contact forces increases linearly in all degrees of freedom, but with different slopes which are defined as the sensitivity.

- By looking at the sensitivities for each joint, it can be observed which uncertainty in a certain joint is contributing the most to the error for a certain trajectory. We observed that the values for the sensitivity are not the same for both trajectories. By altering the joint trajectory, it is thus possible to alter the sensitivity. It could thus be a possibility to use this information to improve the contact force estimation by designing such a joint trajectory that the sensitivity is minimized, but that it is still suitable for performing the task.

- In order to quantify for which magnitude of uncertainty in the Coulomb joint friction, the residual method would still deliver results that are usable, an uncertainty in the Coulomb joint friction is introduced for all 7 joints ranging from -10% to 10%. The mean absolute percentage error is then computed over the complete time interval $t = 0 - 5$ s. It can be observed that an uncertainty of approximately 1% in the Coulomb joint friction leads to a mean absolute percentage error of 10% in the force estimations $\hat{F}_c^x$ and $\hat{F}_c^y$. An uncertainty

of approximately 5% and 3% results in a mean absolute percentage error of 10% for $\hat{F}_z^y$ for trajectory 1 and 2 respectively. Although the margins for error seem to be small for $\hat{F}_c^x$ and $\hat{F}_c^y$ for the trajectories used in this report, the estimation of $\hat{F}_c^z$ is shown to be less sensitive and seems to be the most promising and most suitable for implementation on a physical robot.

Chapter 5

Conclusions and recommendations

5.1 Conclusions

In this report we present the results of the study to the influence of model uncertainty to the estimation of contact forces via the residual method. A simulator is realized in Matlab to perform dynamic simulations of the ULNA arm, which enables visualization of the motion of the robot and to observe the results and behavior of the residual method. We have created two reference trajectories that are resembling the wiping of a table. In particular, we have looked at the influence of the uncertainty in the Coulomb friction parameter in the joints since this is most likely to be uncertain in reality.

- It can be concluded that the residual contact force estimation method is able to estimate contact forces at the end effector with minimal error in the case of no parameter uncertainty. The maximum root mean squared error over the complete time interval $t = 0 - 5$ s is $E_rms = 0.0502$ N. This is the error in $\hat{F}_x$ for trajectory 1 with a simulation step size of $h = 1e - 3$ s and gains $K_i = 1000$.

- When introducing uncertainty in the Coulomb friction parameter in the joints, the residual method directly returns the difference in the error that was made for the Coulomb friction parameter μ_c. With a true Coulomb joint friction parameter $\mu_c = 3$, an uncertainty of 10% leads thus to an error of $0.1 \times 3 = 0.3$ when estimating the external joint torques τ_e.

- The joint trajectory of the robotic arm, influences the sensitivity S. The magnitude of the sensitivity describes how sensitive the residual method is to uncertainties in the Coulomb friction parameter of the joints. The higher the sensitivity, the larger the error will be in the contact force estimation for a certain uncertainty. It can be seen that by changing the joint trajectories, the accuracy of the force estimation can be influenced.

- In order to determine what accuracy should be obtained in order for the contact force estimation to be a usable result, an error of 10% in the force estimation is taken, acting as a rule of thumb.
  It can be concluded that for both trajectories introduced in this report, an uncertainty in the Coulomb joint friction of approximately 1% leads to an error of 10% in the estimation of $\hat{F}_c^x$ and $\hat{F}_c^y$.
  An uncertainty in the Coulomb joint friction of approximately 5% leads to an error of 10% in the estimation of $\hat{F}_c^z$ for trajectory 1, while an uncertainty in the of approximately 3% leads to an error of 10% in the estimation of $\hat{F}_c^z$ for trajectory 2.

In this report, we also present the realization of a force plate for the purpose of validation of contact force estimations, using a 6-DOF force torque sensor. The force plate is able to measure contact forces in all 3 cartesian directions for static contacts and dynamic contacts. An initial calibration procedure to calibrate measurements for contact forces in the z-direction is performed.

- It can be concluded that the force plate is able to estimate contact forces in the z-direction within an accuracy of 0.1 N for loads up to approximately 20 N. Due to the fact that the analysis on the parameter uncertainty has shown much larger errors. It can be concluded that the accuracy in z-direction is sufficient for the purpose of verification of the contact force in this direction.
- It can be concluded that a bias error is present that needs to be corrected. This bias error is changing over time and is most likely affected by noise and changes in the environment.
- It can be concluded that an increase of the load in z-direction of the plate, leads to an increase in the error of the measurements of the forces in x- and y-direction, even though no loads are applied in these directions.

5.2 Recommendations

Based on the previously stated conclusions, the following recommendations are done for the residual method:

- For certain applications it might be desirable that the contact point of the robot is different depending on the task and the joint configuration of the robot. This location of this contact point is then influencing the contact jacobian and thus influencing the contact force estimation. It is recommended to examine the effect of uncertainty in the contact jacobian $\mathbf{J}_c$ and how different types of contact could influence the contact force estimation.
- In order to determine the effect of uncertainty on the contact force estimation for other system parameters, it is recommended to perform simulations in which other various test cases are examined. These cases could for instance be to examine the effect of mass uncertainty.
- It is recommended to further look into the effect of the robot joint trajectory on the contact force estimation, by designing trajectories that minimize the sensitivity to parameter uncertainty. This way it could be possible to minimize the error in the contact force estimation while the trajectory maintains to be suitable for the task specification.
- The residual method directly returns the error in the Coulomb joint friction parameter μ_c. By knowing this it might be useful to use this information to decrease the uncertainty in this parameter by using adaptive control. This way the accuracy of the Coulomb joint friction could improved which eventually improves the contact force estimation.
- For future applications it might be useful to control not only the contact forces but the contact torques as well. Therefore, it is recommended to conduct further research in estimation of the contact torques.

Based on the previously stated conclusions regarding the force plate, the following recommendations are done:

- An increasing load in the z-direction of the force plate leads to increasing errors in the measurement of forces in the x- and y-direction. Since loads in the the x- and y-direction are absent an explanation has to be found for this result. It could possibly be explained by the calibration of the sensor which has been 3 years ago. The manufacturer of the sensor recommends annual recalibration and it is therefore recommended to ship the sensor to the manufacturer for a recalibration procedure.

- It is recommended to use additional filtering to the signal coming from the sensor. This could reduce measurement noise and increase accuracy.
- Due to the mass of the plate it has been observed that contacts with high impacts, lead to vibrations in the plate that disturb the measurements. It is therefore recommended to apply low-impact contacts for verification purposes of the contact force estimation.
- Due to the bias error that is present, the signal coming from the force torque sensor needs to be corrected. Since this bias error changes over time, it is recommended to determine its value as short as possible before performing the measurement.
- It has been observed that attaching the bottom and top plate of the force plate loosely to the sensor, results in errors in the measurements. It is therefore recommended to screw the top and bottom plate **tightly** to the sensor.
- In order to determine the accuracy for measuring contact forces in the x- and y-direction of the force plate, it is recommended to design a calibration procedure for these degrees of freedoms.

References

1. J De Schutter, H Bruyninckx, WH Zhu, MW Spong, Force control: a bird's eye view, Control Problems in Robotics and Automation, 1998.
2. A. De Luca and F. Flacco, Integrated control for pHRI: Collision avoidance, detection, reaction and collaboration, in Proc. IEEE Int. Conf. on Biomedical Robotics and Biomechatronics, 2012, pp. 288 295.
3. E. Magrini, F. Flacco, A. De Luca. Estimation of contact forces using a virtual force sensor. Intelligent Robots and Systems (IROS), IEEE/RSJ International Conference. pp. 2126-2133, 2014.
4. PAL Robotics, Barcelona, Spain, http://pal-robotics.com/en/home/
5. iWholeBodyModel Interface: https://github.com/robotology/mex-wholebodymodel
6. AMTI website, digital image, viewed 25-05-2016, http://www.amti.biz/images/0R6-7-forces-diagram.jpg
7. Roger T. Fenner, J.N. Reddy, Mechanics of Solids, CRC Press, 31 Mar 1991, 648 pages
8. A. De Luca, A. Albu-Schaffer, S. Haddadin, G. Hirzinger. Collision Detection and Safe Reaction with the DLR-III Lightweight Manipulator Arm. in: Intelligent Robots and Systems, 2006 IEEE/RSJ International Conference. pp. 1623 - 1630.
9. Filippo DIppolito, Francesco Alonge and Elisa Cucco. Contact Estimation in Robot Interaction. International Journal of Advanced Robotic Systems, 2014, 11:96. doi: 10.5772/58688.
10. V. van Geffen, A study of friction models and friction compensation, Traineeship report, Technische Universiteit Eindhoven, Department of Mechanical Engineering, December 2009
11. Coefficient of friction for a range of material combinations, static and dynamic, http://www.tribology-abc.com/abc/cof.htm
12. Avanzini, F., Rocchesso, D.: Physical modeling of impacts: Theory and experiments on contact time and spectral centroid. In: Proc. Int. Conf. Sound and Music Computing (SMC06), Paris (2004) 287-293.
13. Waiboer, R., Aarts, R., Jonker, B., Velocity dependence of joint friction in robotic manipulators with gear transmissions, MULTIBODY DYNAMICS, ECCOMAS Thematic Conference, 2005
14. Le-Tien, L., Albu-Schäffer, A., Adaptive Friction Compensation in Trajectory Tracking Control of DLR Medical Robots with Elastic Joints, 2012 IEEE/RSJ International Conference on Intelligent Robots and Systems October 7-12. Vilamoura, Algarve, Portugal, pp. 1149 - 1154, 2012.
15. Chen, C, Friction modeling and experimental identification of a mitsubishi PA10-6CE robot manipulator, MSc Thesis, University of Florida, 2013

16. Chai, T., Draxler, R.R., Root mean square error (RMSE) or mean absolute error (MAE)? Arguments against avoiding RMSE in the literature, Geosci. Model Dev., 7, 12471250, 2014

17. Mark W. Spong, Seth Hutchinson, and M. Vidyasagar, Robot Modeling and Control, Wiley & Sons, January 2004

18. Katharina Kufieta, Force Estimation in Robotic Manipulators: Modeling, Simulation and Experiments, MSc Thesis, Department of Engineering Cybernetics, NTNU, January 29, 2014.

19. A. Stolt, M. Linderoth, A. Robertsson, R. Johansson, Force Controlled Robotic Assembly without a Force Sensor, IEEE International Conference on Robotics and Automation, pp. 1538-1543, 2012

20. L. Dinh Phong, J. Choi, S. Kang, External Force Estimation Using Joint Torque Sensors for a Robot Manipulator, IEEE International Conference on Robotics and Automation, pp. 4507-4512, 2012

21. A. Wahrburg, S. Zeiss, B. Matthias, H. Ding, Contact Force Estimation for Robotic Assembly using Motor Torques, IEEE International Conference on Automation Science and Engineering, Taipei, Taiwan, pp. 1252-1257 ,2014

Appendix A

A.1 Simulation parameters

To determine the influence of the step size h, a short study is done to examine the effect of varying its magnitude. For the forward Euler method, the global error is proportional to the step size. A step size that is too low will thus result in an error that is too large. If the step size is set too high, simulations require a lot of simulation time for little accuracy in return. In Figure A.1, the error in the estimation of the contact force in z-direction is considered as a function of time, for step sizes of $h = 1\text{e}{-2}$ s, $h = 1\text{e}{-3}$ s and $h = 1\text{e}{-4}$ s. The ideal situation is considered in which the observer parameters are equal to the model parameters. The errors that are still occurring in this case, must in theory come from numerical errors or simply due to bad performance of the observer. In this way, the step size that gives the best trade off between simulation speed and performance in the simulations can then be determined.

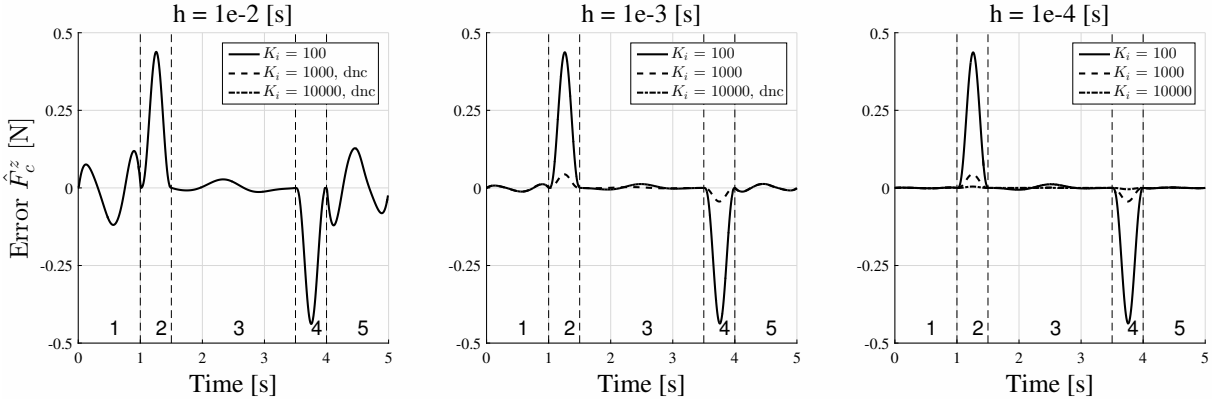

Figure A.1: Error in $\hat{F}_c^z$ for step sizes $h = 1\text{e}{-2}$ s, $h = 1\text{e}{-3}$ s and $h = 1\text{e}{-4}$ s while varying the observer gain entries for $K_i = 100$, $K_i = 1000$ and $K_i = 10000$

Besides the step size, the simulation parameter that has to be considered are the values in the diagonal observer gain matrix $K_I > 0$ in (2.5), which has direct influence on the performance. These values are ideally as high as possible, although values that are too high will result in numerical instabilities. Figure A.1 shows the error of $\hat{F}_c^z$ for different values of the gain entries K_i in the gain matrix K_I.

The first thing that can be observed from Figure A.1, is that increasing the step size leads to a smaller error in trajectory parts 1, 3 and 5. Looking at section 4.1, it can be seen that in these trajectory parts the robot is making large movements. Increasing the step size will thus lead to a smaller error in these parts.

The second thing that can be observed, is the influence of increasing the entries K_i in observer gain

matrix K_I, which are set to $K_i = 100$, $K_i = 1000$ and $K_i = 10000$. For a step size of $h = 1e{-}2$ s, it can be seen that the observer only converges to a solution for $K_i = 100$. Setting K_i to a higher values will not result in a converged solution.
For a step size of $h = 1e{-}3$ s, it can be seen that increasing the observer gain does not influence the error on trajectory parts 1, 3 and 5. It does however influence the error in trajectory parts 2, 3 and 4, in which the arm is interacting with the environment. It again holds that when the entries K_i are set too high, that the solution does not converge which is the case when $K_i = 10000$.
Finally, for a step size of $h = 1e{-}4$ s, the improved performance of the solution can be observed with an even smaller error in trajectory parts 2, 3 and 4.

It can thus be concluded that for obtaining accurate results in the case of the arm moving in space, a higher step size will result in a smaller error. In the case of the arm interacting with the environment, higher values of K_i will result in smaller errors. For the simulations in this report the step size is set to $h = 1e{-}3$ s with observer gains of $K_i = 1000$ to obtain a well enough trade off between simulation time and accuracy.

Since the Euler method is a relatively basic method to solve differential equations numerically, it could be considered to use a more advanced solver for implementation on a real robot. Real robots usually have a limited frequency with which data can be obtained, which limits the observer step size h. A more advanced solver could then be a solution to get more accurate results for the same step size.

Appendix B

B.1 Force plate experiments

In figure B.2, the results of the for a straight line wiping motion with a plastic objects are shown, which is intended to mimic the motion of the end effector of the robot in Chapter 4. A schematic representation of this trajectory can be seen in figure B.1. The plastic rod was brought in contact with the plate at around $t = 10$ s, after which it is moved in a straight line diagonally while maintaining contact with the plate. Notice the dependency of the surface friction F_x and F_y on the normal force F_z by all of them having similar profiles. Besides this, it is interesting to notice the disturbances caused by vibrations which are best captured in the torque measured in z-direction.

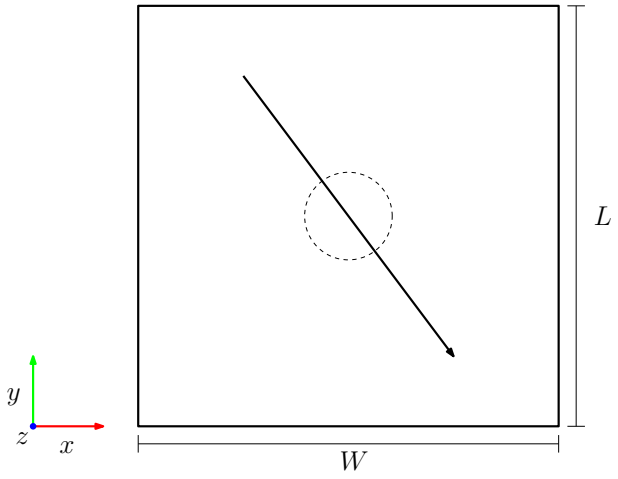

Figure B.1: Trajectory mimicking the simulation trajectory in Chapter 4 with a plastic rod

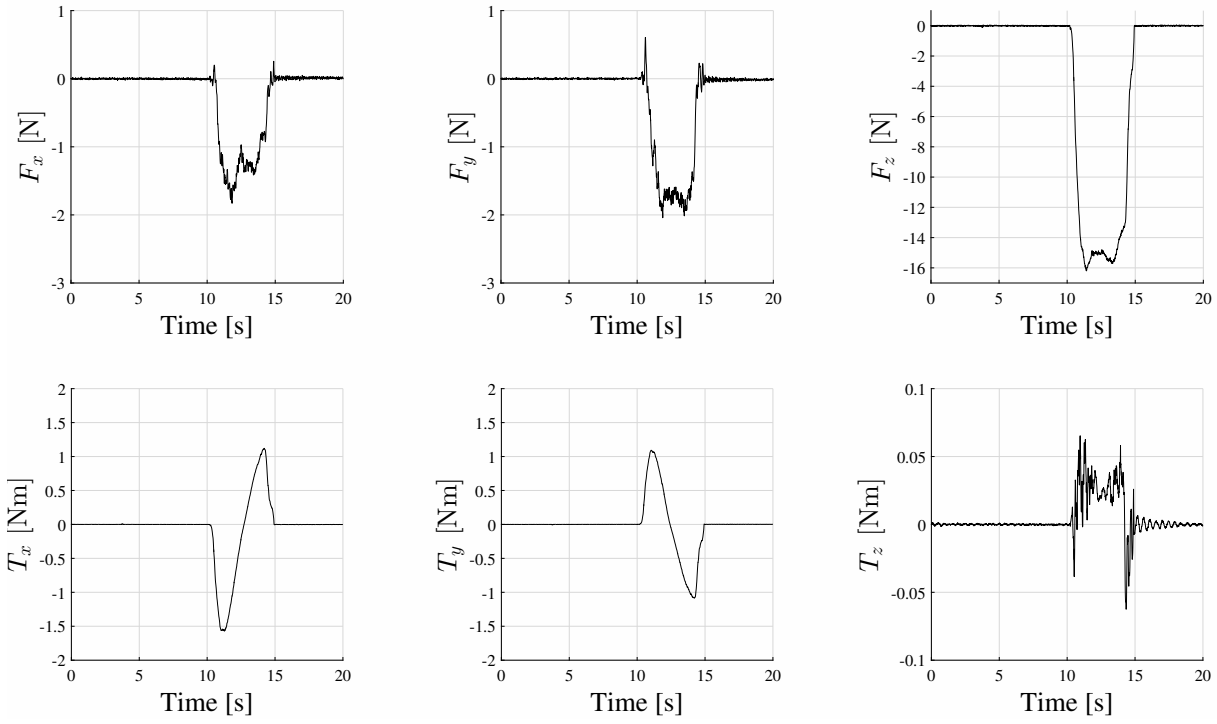

Figure B.2: Measured contact forces and torques for mimicking the simulation trajectory in Chapter 4

Figure B.4 shows the results of a circular wiping motion on the plate with a sponge, while following the trajectory shown in figure B.3. Notice the sinusoidal profiles of the results in all degrees of freedom.

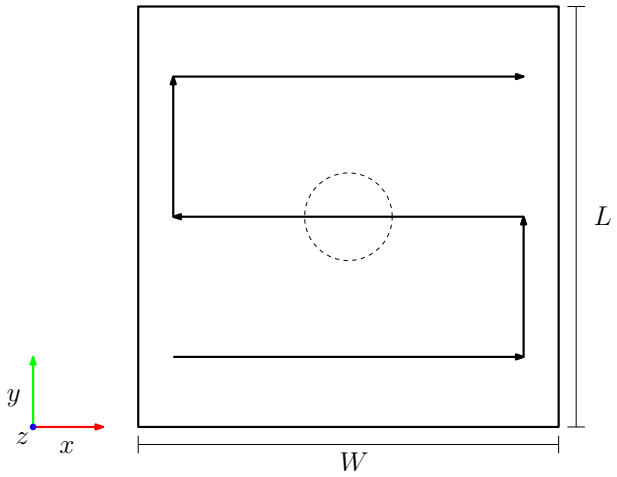

Figure B.3: Trajectory for which a wiping motion trajectory with a sponge is performed

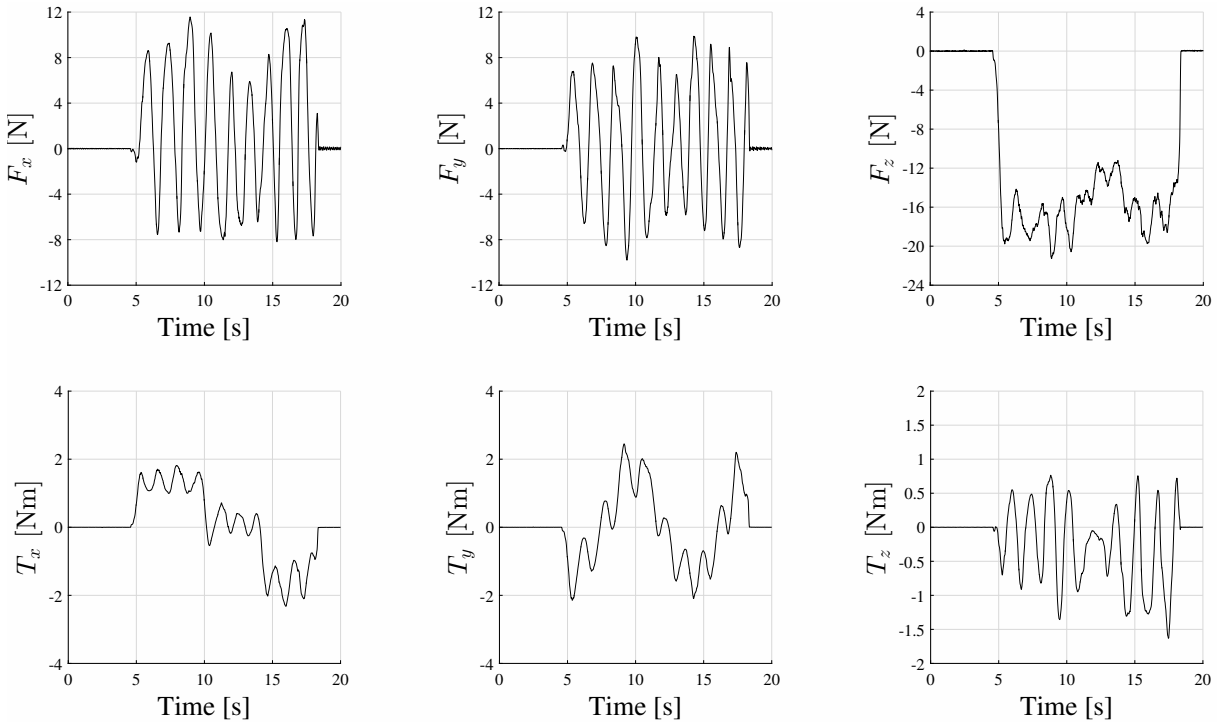

Figure B.4: Measured contact forces and torques for a circular wiping motion

In order to obtain results in case of a small contact force, a sheet of paper is attached to the force plate after which the word "ULNA" is written on the sheet with a marker as shown in figure B.5. The results of this experiment can be seen in figure B.6. Notice the peaks that are visible most clearly for F_z, which represent the marker hitting the plate in order to draw a new line. Also notice that due to the fact that contact forces are small, that they approach the level of the noise.

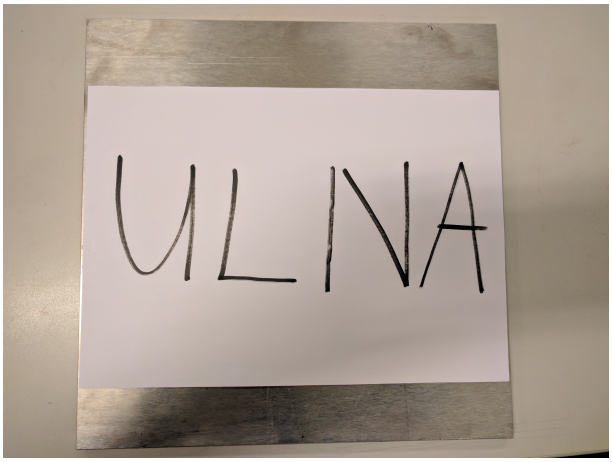

Figure B.5: Writing the letters "ULNA" on a sheet of paper

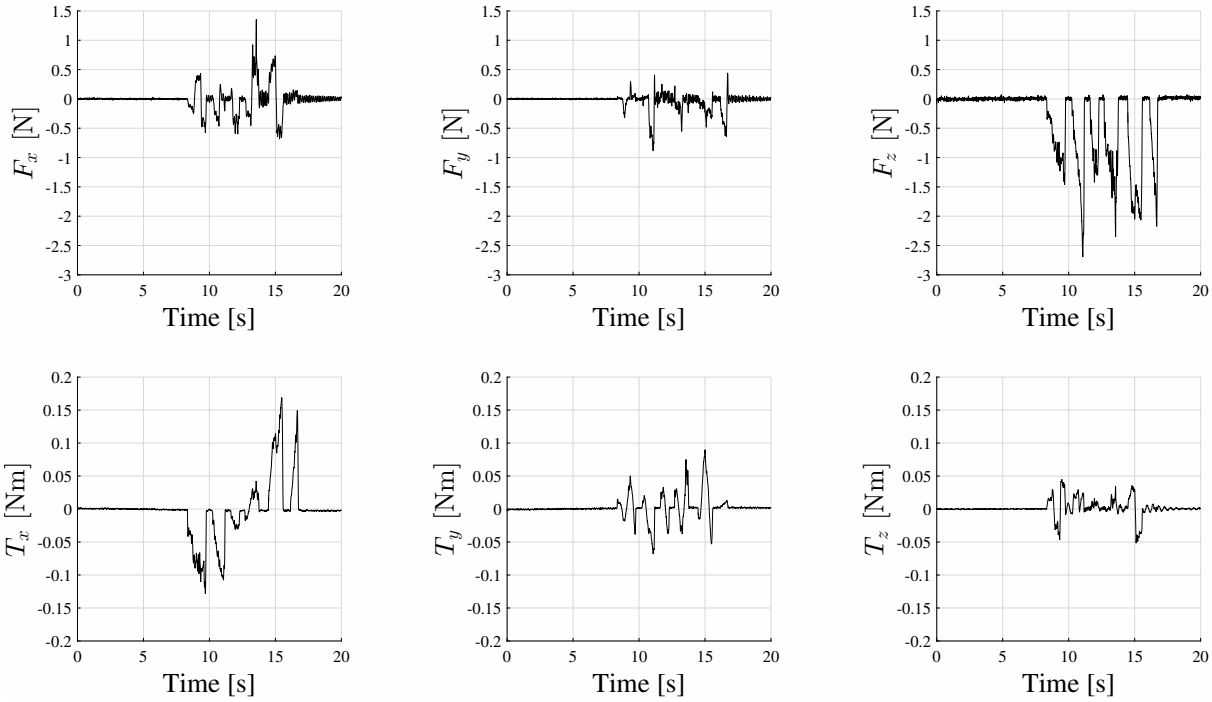

Figure B.6: Measured contact forces and torques for writing the Letters "ULNA"